Evolution of deep-sea sediments across the Paleocene-Eocene and Eocene-Oligocene boundaries

Bridget S. Wade[a], James F. O'Neill[a, b], Chawisa Phujareanchaiwon[a, c], Imran Ali[a, d], Mitchell Lyle[e] and Jakub Witkowski[f]

[a] *Department of Earth Sciences, University College London, Gower Street, London, WC1E 6BT, UK*

[b] *Department of Geography, King's College London, Bush House (NE wing), 30 Aldwych, London, WC2B 4BG, UK*

[c] *Department of Geology, Chulalongkorn University, 254 Phayathai Rd, Khwaeng Pathum Wan, Khet Pathum Wan, Bangkok 10330, Thailand*

[d] *PetroStrat Limited, Tan-y-Graig, Parc Caer Seion, Conwy, North Wales, LL32 8FA, UK*

[e] *College of Earth, Ocean, and Atmospheric Science, Oregon State University, 104 CEOAS Admin Bldg, Corvallis, Oregon 97331, USA*

[f] *Institute of Marine and Environmental Sciences, University of Szczecin, ul. Mickiewicza 16a, 70-383 Szczecin, Poland*

ABSTRACT

The composition and distribution of deep-sea sediments is the result of a multitude of climatic, biotic and oceanic conditions relating to biogeochemical cycles and environmental change. Here we utilize the extensive sediment archives of the International Ocean Discovery Program (IODP) and its predecessors to construct maps of deep-sea sediment type across two critical but contrasting boundaries in the Paleogene, one characterised by an interval of extreme warmth (Paleocene/Eocene) and the other by global cooling (Eocene/Oligocene). Ocean sediment distribution shows significant divergence both between the latest Paleocene and Paleocene Eocene Thermal Maximum (PETM), across the Eocene-Oligocene Transition (EOT), and in comparison to modern sediment distributions. Carbonate sedimentation in the latest Paleocene extends to high southern latitudes. Disappearance of carbonate sediments at the PETM is well documented and can be attributed to dissolution caused by significant ocean acidification as a result of carbon-cycle perturbation. Biosiliceous sediments are rare and it is posited that the reduced biogenic silica deposition at the equator is commensurate with an overall lack of equatorial upwelling in the early Paleogene ocean. In the Southern Ocean, we attribute the low in biosiliceous burial, to the warm deep water temperatures which would have impacted biogenic silica preservation. In the late Eocene, our sediment depositional maps record a tongue of radiolarian ooze in the eastern equatorial Pacific. Enhanced biosiliceous deposits in the late Eocene equatorial Pacific and Southern Ocean are due to increased productivity and the spin-up of the oceans. Our compilation documents the enhanced global carbonate sedimentation in the early Oligocene, confirming that the drop in the carbonate compensation depth was global.

***Keywords*:** Sediments; carbonate compensation depth; PETM; Eocene/Oligocene boundary; silica; dissolution

1. Introduction

Deep-sea sediments represent the most widespread and complete record of Cenozoic oceanic and climatic state. The pattern and composition of seafloor sediments seaward of the continental shelf is a reflection of biological, geochemical, terrestrial and climatic conditions on Earth at the time of deposition (Chester and Jickells, 2012). Sedimentary changes through the geological record are an essential tool in reconstructing past conditions on Earth, constraining key changes in the atmosphere-ocean system and facilitating the characterization of significant climatic perturbations. As such, the study of paleo-sediment records facilitates the examination of broad scale oceanic and climatic changes including but not limited to ocean productivity, carbonate chemistry, and glacial processes.

The overall purpose of this study was to examine the distribution of seafloor sediments as the Earth transitioned from the warm conditions of the late Paleocene to the icehouse conditions of the early Oligocene. We created a compilation of all major deep sea sediments across two major climate transitions, the PETM and EOT. We aimed to determine how palaeoceanographic phenomena were reflected in the sediment pattern of these two critical and contrasting climate intervals, and explore how and why the distribution in the Paleogene differs to the modern.

Over the past half century, the International Ocean Discovery Program (IODP) and its predecessors have cored deep-sea sediments throughout the oceans, resulting in an ever growing archive of paleoclimatological data. Here we collate and synthesize data from deep-sea archives from over 175 DSDP/ODP/IODP sites (up to IODP Expedition 362) and present a compilation of global ocean sediment distribution maps. We concentrate on four time intervals; latest Paleocene (~57-56 Ma), PETM (~55.9 Ma), latest Eocene (~34 Ma) and earliest Oligocene (~33.5 Ma). The tables provide a catalogue of all existing ocean drilling sites covering these intervals drilled to date. In mapping ocean sediment distribution for the upper Paleocene, PETM, upper Eocene and lower Oligocene, this study has produced a functional visual resource in understanding the biogeochemical change and oceanic response to climate perturbations. These maps provide a record of sedimentary changes on a global scale across major climate transitions to compare with the sediment distribution in the modern oceans, and contribute to the understanding of environmental change across two critical intervals in the

Paleogene. We review the global implications of paleoclimate on ocean sedimentation and the impact of changes in ocean dissolution and productivity.

1.1 Modern global distribution of marine sediments

Knowledge of modern sediment distribution in the global ocean and its controls provide a better understanding of global biogeochemical cycles and response of marine sediment to environmental and climatic changes. Oceanography and marine geology textbooks generally contain a map of the global oceanic sediment distribution (e.g., Davies and Gorsline, 1976; Barron and Whitman, 1981; Hüneke and Mulder, 2011), which normally illustrates five or six main types of sediments in the ocean basins based on their primary composition and provenance. Modern sediment distribution in the ocean is determined by the sediment sources, as well as the physical and chemical factors that control deposition.

Marine sediments can be divided into two main categories, lithogenous and biogenous (Lyle, 2014). Lithogenous sediments derive from weathering and erosional processes on land and underwater, including submarine volcanoes and consist of terrigenous sediments, glacial sediments and deep-sea/red clays. Most prominent are river-borne sediments that form voluminous deposits near land. Glaciomarine sediments include glacially transported sediments, such as ice-rafted debris. In the modern oceans, glaciomarine sediments occupy high latitude areas, especially the margins around Antarctica and in the North Atlantic (Fig. 1). Aeolian sediments/deep-sea clays generally accumulate below a depth of ~5,000 m in the modern ocean (Chester and Jickells, 2012). They cover large areas of the ocean where sedimentation rates are low and where only windblown dust can accumulate. Volcanic ash can be locally important near island arcs.

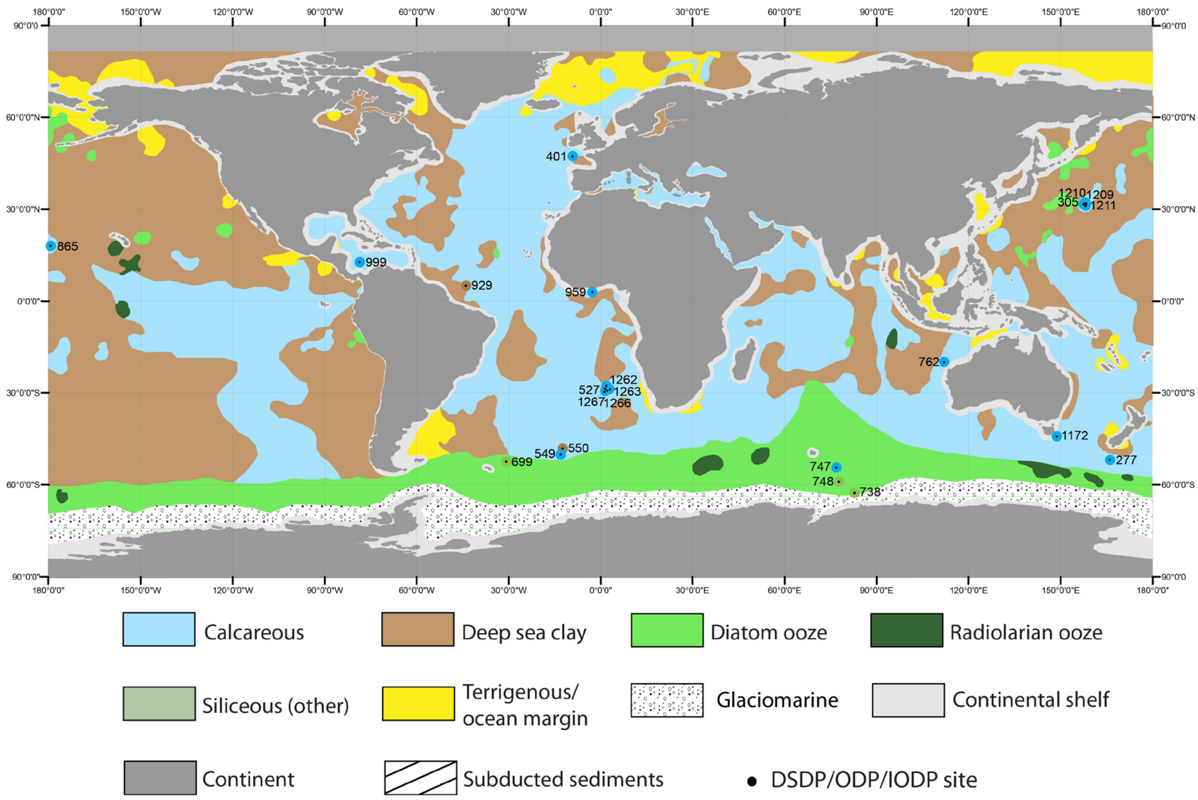

Figure 1. Modern distribution of ocean sediment (based on Davies and Gorsline, 1976; Leinen et al., 1989; Chester and Jickells, 2012; Dutkiewicz, et al., 2015). For reference we include DSDP/ODP/IODP sites that also have both a Paleocene/Eocene and Eocene/Oligocene boundary.

Biogenous sediments, often referred as oozes, are produced from biotic processes and composed of calcareous and siliceous microfossils. A primary control on biogenic sedimentation is ocean productivity which impacts the types and distribution of marine organisms, and the rate of fossil test production and deposition. Biogenic sediments are also subject to dissolution, which affects carbonate and silica preservation and further shapes the areal coverage of the deposit. Major climate changes can have a crucial impact on marine biodiversity and dissolution, resulting in different oceanic sediment patterns.

Calcareous oozes are a major component of deep-sea sediments which originate from calcareous micro-organisms, mainly from planktonic foraminifera and calcareous nannofossils. The distribution of calcareous sediments in the ocean is principally controlled by the depth of the lysocline and carbonate compensation depth (CCD), which reflects the chemistry of the ocean carbonate system (Chester and Jickells, 2012). Maximum dissolution occurs below the lysocline, and beneath the CCD sediments are carbonate free (Takahashi and Broecker, 1977). The CCD varies in each ocean basin; the modern CCD in the Pacific is ~3,500-5,000 m, and in the Atlantic and Indian ocean is 4,500-5,000 m (Berger et al., 1976; Chester and Jickells, 2012).

Siliceous oozes are composed of siliceous skeletal remains derived mainly from diatoms and radiolarians. In the modern ocean, biosiliceous dominated sediments are mainly focused in a few distinct areas, particularly in the Southern Ocean (diatom oozes), and equatorial Pacific (mixed carbonate-opal biogenic sediments) (Fig. 1). The distribution of siliceous sediments is primarily controlled by productivity and dissolution (Chester and Jickells, 2012; Ragueneau et al., 2000). A positive relationship has been shown between areas of high productivity and siliceous sediment accumulation (Calvert, 1974; Garcia et al., 2010; Barron and Baldauf, 1989). It has also been shown that aluminium concentrations also impact the degree of biogenic silica preservation (DeMaster, 2014). Preservation of siliceous organisms in modern ocean sediments is very low (1-5%) compared to the production rate in surface waters as the oceans are undersaturated in silica at all depths (Siever, 1957; Calvert, 1974; Ragueneau et al., 2000; Barron et al., 2015).

Sediment deposition on the ocean floor is not a simple reflection of productivity in surface waters as it involves many factors (Hüneke and Henrich, 2011). Dutkiewicz et al. (2015) produced the first digital map of modern oceanic sediments showing that distribution of seafloor sediment lithology is more complicated than the earlier hand-drawn maps and biogenic sediments show a strong relationship with sea surface nutrients, salinity and temperature.

1.2 Paleocene Eocene Thermal Maximum

The PETM (55.93–55.71 Ma; Westerhold et al., 2017) represents a short-lived but dramatic hyperthermal event, characterised by a >2‰ negative carbon isotope excursion in marine and terrestrial sections (Kennett and Stott, 1991; Koch et al., 1992; Dickens et al., 1995; Zachos et al., 2005; Dickens, 2011). Although the mechanism is still debated, the PETM is thought to have resulted from a multi-pulsed release of ^{13}C depleted carbon into Earth's exogenic carbon reservoir (Zeebe et al., 2009; Bowen et al., 2015; Frieling et al., 2016). The addition of thousands of petagrams of carbon (Meissener et al, 2014) to the ocean-atmosphere system had a profound effect on physical, geochemical and biotic processes on Earth. Ocean temperatures increased significantly, with average SSTs increasing by ~4ºC or more (Dunkley Jones et al., 2013; Frieling et al., 2017) and deep ocean temperatures increasing by ~6ºC (Kennett and Stott, 1991). Surface ocean pH decreased by 0.3 pH units whilst the lysocline and CCD shoaled by >2 km (Zachos et al., 2005; Penman et al., 2014; Bralower et al., 2018). Increased atmospheric warming, against a late Paleocene world with atmospheric CO_2 concentrations hundreds of ppmv greater than today and ice-free poles, resulted in a reduced latitudinal temperature gradient, weakening of the trade winds, significant alteration to the rate and nature of meridional overturning circulation and an overall decrease in ocean ventilation and nutrient availability (Winguth et al., 2012; Pälike et al., 2014; Heinze and Ilyina, 2015). On the seafloor benthic foraminifera suffered a major extinction, with 35-50% of species affected (Kennett and Stott, 1991; Thomas and Shackleton, 1996).

1.3 Eocene-Oligocene Transition

The Eocene-Oligocene Transition (EOT; ca. 34–33Ma) is one of the most significant episodes of climatic change in the Cenozoic. Through the Eocene the global climate developed from a warm, ice-free "greenhouse" world to the glacial Antarctic "icehouse" of the Oligocene. Benthic foraminiferal oxygen isotope records show a rapid positive excursion across the EOT (e.g., Kennett and Shackleton, 1976; Miller et al., 1991; Zachos et al., 1996; Coxall et al., 2005; Katz et al., 2008), reflecting the establishment of continental-scale Antarctic ice sheets. Increased ice volume is additionally indicated by ice-rafted debris in the Southern Ocean and a major drop in global sea level (Kennett and Shackleton, 1976; Miller et al., 1991, 2008a, b; Zachos et al., 1996; Schulte et al., 2009). Across the EOT there was a rapid and permanent deepening of the CCD (van Andel and Moore, 1974; Heath et al., 1977; Lyle et al., 2002; Coxall et al., 2005; Pälike et al., 2012), terrestrial and marine cooling (Zanazzi et al., 2007; Wade et al., 2012), and biotic turnover (Prothero and Berggren, 1992; Dunkley Jones et al., 2008; Pearson et al., 2008; Wade and Pearson, 2008; Wade et al., 2018; Houben et al., 2019a). The causal mechanisms are a decrease in atmospheric CO_2 below a critical threshold (Pearson et al., 2009), coupled with orbital forcing (Pälike et al., 2006).

2. Methodology

2.1 Data Compilation

Sediment data (Tables 1-3) were sourced from the archives of the International Ocean Discovery Program (IODP) and its predecessors (Deep Sea Drilling Project, DSDP; Ocean Drilling Program, ODP; Integrated Ocean Drilling Program, IODP) representing over 50 years of ocean sediment core sampling and a significant repository of primary geological data. To identify DSDP/ODP/IODP sites with a sedimentological record covering the study intervals (late Paleocene / early Eocene and late Eocene / early Oligocene), a review of literature was performed, with shipboard data for sites referenced therein compiled. To identify the target intervals, we used all geochronological information available, including calcareous and siliceous biostratigraphy, magnetostratigraphy and stable isotope stratigraphy, though there are very few sites where all information is available.

The PETM was identified at sites either by the Shipboard Scientific Party or by referral to post cruise literature (e.g., Kelly et al., 2012; Hollis et al., 2015; Frieling et al., 2019; Penman et al., 2019; Witkowski et al., 2020a). To detect the PETM interval in cruise reports predating its recognition as a significant global climatic perturbation (chiefly DSDP/ODP sites cored prior to 1991), the Paleocene/Eocene boundary was identified through plankton biostratigraphy, and/or the benthic foraminiferal extinction. In a number of sites cored before 1991, subsequent investigations have re-examined core samples to obtain $\delta^{13}C$ values and established the position of the negative carbon isotope excursion (CIE). Such sites are also included in our dataset. For the late Paleocene, we targeted the interval from 57 to 56 Ma. At sites with a carbon isotope stratigraphy, we selected the interval prior to the CIE (~56 Ma), providing that stratigraphic control indicated that sedimentation was continuous.

The DSDP, ODP and IODP sites that contain sedimentary records of EOT are primarily identified based on the scientific literature. Only sites that contain complete sections spanning the Eocene-Oligocene boundary without hiatuses are used, as confirmed by age-depth models (e.g., Firth et al., 2013; Houben et al., 2019b; Witkowski et al., 2020a). Several ocean cores covering the Eocene-Oligocene boundary are incomplete or condensed, for example DSDP sites 216, 217, 460, and ODP sites 689, 742, 752, 758 and 1172 (Houben et al., 2019b). Hiatuses across the EOT have been attributed to an increase in ocean circulation vigour and glacioeustatic sea-level fall associated with the climate shift (Kennett and Shackleton, 1976; Zachos et al., 1996; Miller et al., 2008a, b, 2009; Houben et al., 2019a). However, it is possible that some hiatuses were not detected due to poor geochronological records. As the Eocene-Oligocene boundary was formally defined in 1993, the Eocene-Oligocene boundary in the ocean drilling site reports prior to 1993 is identified from the biostratigraphy (e.g., Wade et al., 2011). There are uncertainties about the boundary in some sites owing to lack of marker fossils. For the late Eocene, we targeted the calcareous nannofossil CP15/CP16 (NP19-20/NP21) zonal boundary (~34 Ma), within Chron C13r. For the early Oligocene at sites with an oxygen isotope stratigraphy, we selected the interval at the start of the early Oligocene glacial maximum (~33.5 Ma), corresponding to Chron C13n, and low latitude radiolarian RP19/RP20 zonal boundary.

Sections that are condensed were included in our data set (e.g., EOT at ODP Site 1217), but incomplete sections due to hiatuses, core gaps, significant drilling disturbance and poor recovery are excluded (e.g., PETM at DSDP sites 152, 215, 259, 313, 316, 464, 524, 528, 529, 530, 576, 577, 596, ODP sites 634, 698, 699, 738, 807, 869, 1050, 1183, 1217, 1257 and IODP Site U1407). Site 1051 is retained, although it should be noted that previous studies have suggested that the PETM at this site is incomplete (Farley and Eltgroth, 2003; Röhl et al., 2003; Nicolo et al., 2007). Site 327 was also retained in this study, though siliceous sedimentation ceased ~56.3 Ma (Witkowski et al., 2020a). These data from DSDP, ODP and IODP drilling sites were collected and organized using spreadsheets (Tables 2 and 3) in order to produce comprehensive ocean sediment maps. Our data set provides an inventory of all ocean drilling sites covering these two critical boundaries. The ocean sediment distribution maps are based on 46 sites for the PETM and 175 sites for the EOT (Tables 2 and 3).

2.2 Sediment Classification

To determine the dominant sediment type, the lithologies were examined using barrel sheets, visual core descriptions and smear slide data reported by shipboard scientists. These were compared and corroborated to ensure correct identification of major sediment components for each site across the PETM and EOT interval. The sediment classification in this study adopts a simplified version of the scheme proposed by Mazzullo et al. (1988), which is the standard classification used by the DSDP, ODP and IODP. Sediments are classified based on their major component as recorded in shipboard data archives. Where sediments are described with modifiers they are classified based on the major modifier. An example of this would be ‘nannofossil chalk’, wherein ‘nannofossil’ acts as the major modifier, indicating nannofossils as the dominant sediment component, before the principle name, chalk, indicating calcareous composition and degree of consolidation (Mazzullo et al., 1988).

Five main types of sediments are classified and used in sedimentary maps in this study. The sediments are classified as calcareous, siliceous, clay, siliciclastic and glaciomarine sediments. Calcareous sediments include foraminiferal and nannofossil oozes/chalk/limestone. Siliceous sediments include radiolarian and diatom oozes, chert and porcellanite which represent dense siliceous sediments. Clay consists of sediment (<2 μm), including claystone. Siliciclastic sediments generally consist of sand, silt and mud. Diamictite represents the glaciomarine sediments. The details of sediment classification can be found in Tables 1-3.

Where carbonate sediments are reported as indurated, such as chalk or limestone, these are mapped as oozes if a major biogenic sediment component is indicated. This is a reflection of the notion that lithification occurred largely as a post-depositional process, and that when they were deposited, they would have been poorly consolidated calcareous sediments(oozes) (Chester and Jickells, 2012). Similarly, where the suffix ‘stone’ is used in shipboard rock descriptions to indicate lithified siliclastic sediments (Mazzullo et al., 1988), this is disregarded on the sediment maps and claystone becomes clay. Porcellanite and chert are derived from biogenic opal, and are considered to be the diagenetic transformation of biosiliceous oozes. However, we continued to distinguish radiolarian and diatom ooze from porcellanite and chert on the maps and tables, as the nature of the original biosiliceous deposition (diatom versus radiolarian ooze) is unknown.

2.3 Mapping sediment distributions across critical Paleogene climate transitions

The sediment distribution maps are produced based on sedimentary records from ocean drilling sites. To accurately reconstruct paleogeographies of tectonic plates and locations of drilling sites, GPlates (http://www.gplates.org; Boyden et al., 2011) open source plate reconstruction software was used in conjunction with a dynamic plate reconstruction model (Seton et al., 2012 and references therein). Ocean drilling sites were created as individual features in GPlates and positioned based on present-day longitude and latitude. Specific plate IDs were assigned in line with the defined topology in Seton et al. (2012). A reconstruction was then performed from 56 and 34 Ma to produce a base map onto which sediment distribution could be mapped. The ArcGIS software was used to create site labels and graticules, and the sedimentary maps were drawn using Adobe Illustrator CS4 vector based graphics software. In our paleogeographic maps for the late Eocene and early Oligocene, the Drake Passage is open.

2.4 Sediment extrapolation

As well as mapping sediments based on recorded lithologies for individual drilling sites, some sediment types are extrapolated. The paleobathymetry of the ocean basin model from Muller et al. (2008) (http://www.earthbyte.org), early Paleogene reconstructions of paleobathymetry (He et al., 2019), and the CCD records from literature are used to infer the calcareous depositional areas. This was achieved by comparison with reconstructed positions of mid-ocean ridges, as these by their nature represent areas of significant elevation above the seafloor. As the primary control of carbonate sediment distribution is deposition above the CCD, sediments of this type could be extrapolated along mid ocean ridges with medium confidence for the late Paleocene. For the PETM sediment map, carbonate sediments are not extrapolated to reflect PETM dissolution. Conversely, as clays dominate sediments deposited below the CCD, clays are inferred as the major sediment type on abyssal plains.

Carbonate sedimentation is extrapolated for the EOT based on a CCD depth in the late Eocene of approximately 3,700 m in the Pacific Ocean (Pälike et al., 2012), with the magnitude of deepening across the EOT of more than 1 km (van Andel, 1975; Rea and Lyle, 2005; Pälike et al., 2012). Specifically, the Pacific CCD deepened to 5,000 m in Pacific equatorial regions (van Andel, 1975; Heath et al., 1977), in the Indian Ocean from ~3,600 to 4,000 m (Rea and Lyle, 2005), and in the South Atlantic, evidence from DSDP Legs 73 (Hsü et al., 1984) and 74 (Moore et al., 1984) indicates the CCD dropped from ~3,300 m to 4,300 m. Siliciclastic sediments are extrapolated in the areas near the continents.

A hindrance to complete characterization of sediment distribution arises from biases in the locations and distribution of ocean drilling sites, because paleoceanographic drilling expeditions preferentially target carbonate rich sediments. Large areas of the Southern Ocean, South Pacific, central North Pacific and Arctic Oceans remain virtually un-sampled. In addition, the paleobathymetry map for extrapolation in the Paleogene is of poor resolution. In the context of the limited data available however, this study was designed to present a picture of Paleogene sediment distribution. The pattern of sediment distribution in our maps is a simplified version based on primary controls and data availability, and inevitably under-represents the complexity of sediment deposition, as shown in the modern seafloor map of Dutkiewicz et al. (2015). Many locations show a different lithology to a nearby site, due to the scale of maps and heterogeneous ocean floor conditions (such as varying topography).

3. Results

3.1 Upper Paleocene sediment distribution

On upper Paleocene sediment map (Fig. 2) carbonate sediments dominate the sites sampled, which are predominately on topographic highs, and clay is the principal sediment elsewhere. Of the 46 DSDP, ODP and IODP drilling sites for which the PETM was recovered, only six sites (sites 327, 959, 1171, 1208, M0004, U1403), have non-carbonate dominated sediment immediately prior to the onset of the PETM. With the exception of the Arctic basin, all major ocean basins show evidence of regional carbonate deposition. The majority of carbonate sediments are dominated by nannofossil oozes, with generic calcareous oozes the second most abundant carbonate sediments, and a minor component of foraminiferal oozes recorded. Siliceous sediments are rare; radiolarian ooze is recorded only at Site 327, porcellanite at Site 959, and no diatomaceous oozes are present in the sampled data. In terms of southern hemisphere carbonate sedimentation, there appears to be no latitudinal constraints on sediment deposition, with nannofossil oozes recorded as far south as Site 690 in the Weddell Sea, although, Site 1172 on the East Tasman rise, is dominated by clayey siltstone. The only ocean basin lacking in carbonate sedimentation in the late Paleocene is the Arctic, though with only one site sampled (Site M0004), it is difficult to conclusively say whether the clay sediment at this site represents a regional feature or an anomalous data point. Site U1403, located in the central North Atlantic Ocean, is also dominated by clay across the interval of study. In the western Pacific Ocean Site 1208, located near the modern-day Shatsky rise, displayed a dominant sediment fraction of clay just prior to the PETM. Other western Pacific sites located near the modern-day Shatsky rise (Sites 305, 1209, 1210, 1211 and 1212) are nannofossil ooze dominated in the late Paleocene. Sites 1215, 1220 and 1221 in the equatorial eastern Pacific are all carbonate dominated, as are the sediments at sites 1001 and 999 in the Caribbean Sea. Seafloor sediments at sites 929, 1258, 1259, 1260 in the equatorial to tropical Atlantic Ocean are chiefly nannofossil oozes in the late Paleocene. In the north east Atlantic Ocean, sites 549 and 550, on the western edge of the Goban spur are dominated by nannofossil ooze; whilst Site 401, located in the Bay of Biscay in the early Paleogene, had a sedimentary cover of calcareous ooze in the late Paleocene. Carbonate deposits were added to the maps across parts of the peri-

Tethys region for the late Paleocene (Ouda et al., 2016; Luciani et al., 2007; Alegret et al., 2009; Zhang et al., 2013; Heinze and Ilyina, 2015).

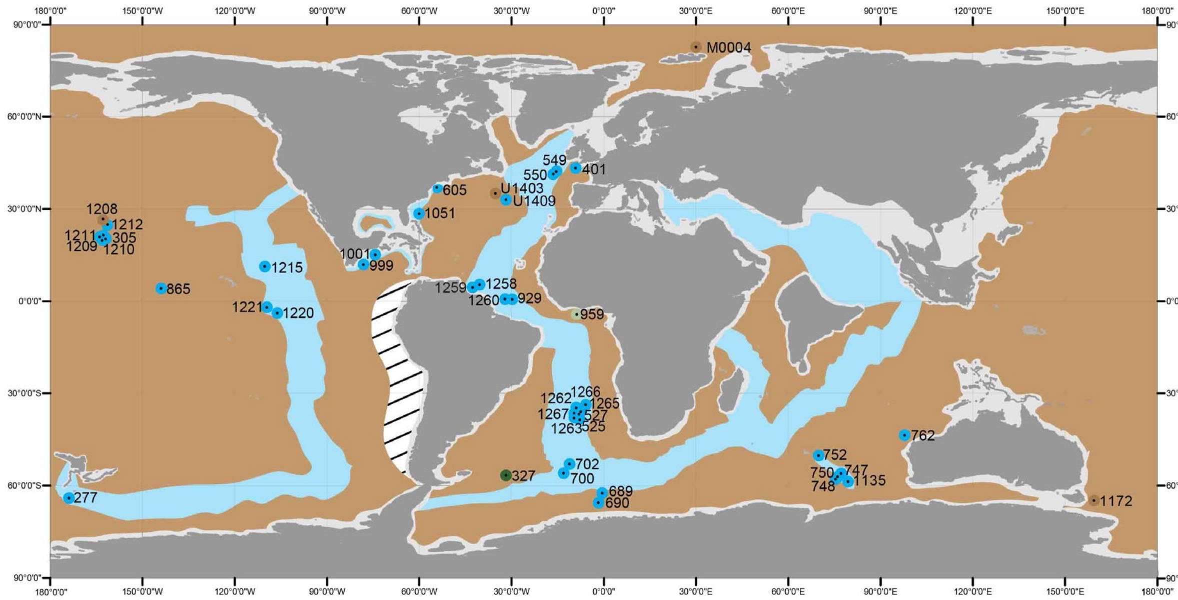

Figure 2. Ocean sediment distribution for the late Paleocene (key as in Figure 1). Carbonate sediments (blues) were abundant across all latitudinal ranges in the late Paleocene, and have been inferred to extend along submarine relief features including mid ocean ridges and Tethys regions (Ouda et al., 2016). In the late Paleocene only one site (Site 327) has a dominant biosiliceous sediment component. Paleobathymetry and the locations of ocean ridges were constrained using Muller et al. (2008) and He et al. (2019).

3.2 PETM sediment distribution

The PETM map (Fig. 3) represents a major shift in sediment component from upper Paleocene nannofossil ooze to PETM clay. This is clearly shown in southern Atlantic sites 525, 527, 1262, 1263, 1265, 1266 and 1267. Sites 689, 690 and 700 in the South Atlantic and Site 605 in the North Atlantic however, remain nannofossil ooze. Siliceous sedimentation (radiolarian ooze) ceased at ~56.3 Ma at Site 327 (Witkowski et al., 2020a) and was overlain by clay. In the tropical to equatorial Atlantic Ocean, sites 929, 1258, 1259 and 1260 also record a transition from nannofossil oozes in the late Paleocene to clay and, in the Caribbean Sea, sites 999 and 1001 record diminished carbonate deposition and a switch to clay as the dominant sediment fraction. Equatorial Pacific sites 1215, 1220 and 1221 record a comparable reduction in carbonate deposition, with clays deposited during the PETM. However, at Site 865, to the northwest of sites 1220 and 1221, deposition of foraminiferal oozes persisted across the PETM, and at sites 305, 1210, 1211 and 1212, a major change in sediment type is not recorded, with these sites remaining nannofossil ooze-dominated. Shatsky Rise (Site 1209) changes from nannofossil ooze-dominated to clay-dominated, whilst the predominance of clays as the major lithology at Site 1208 persisted across the PETM. North Atlantic Site 1051 consists of siliceous carbonate chalk in both the upper Paleocene and PETM, and in the northeast Atlantic Ocean, sediments at sites 401, 549, 550 and U1409 consist predominately of clay throughout this interval; Site U1403, like Site 1208, remains clay-dominated. At site M0004 in the Arctic Basin, clays persisted as the major sediment component across the PETM. The southern Indian Ocean and proto-Southern Ocean sites 750, 752, 762 and 1135 appear to be least affected in terms of carbonate dissolution, and all remained nannofossil ooze-dominated across the PETM, though nearby Site 747 shifted from nannofossil chalk to claystone. Site 1172 on the East Tasman rise remained silt-dominated across the PETM, whilst Site 277 in the southwestern Pacific records majority carbonate deposition at the PETM. High southern latitude sites 702 and 748 transition from chalk to chert across the PETM, and Site 959, in the east Atlantic remains porcellanite.

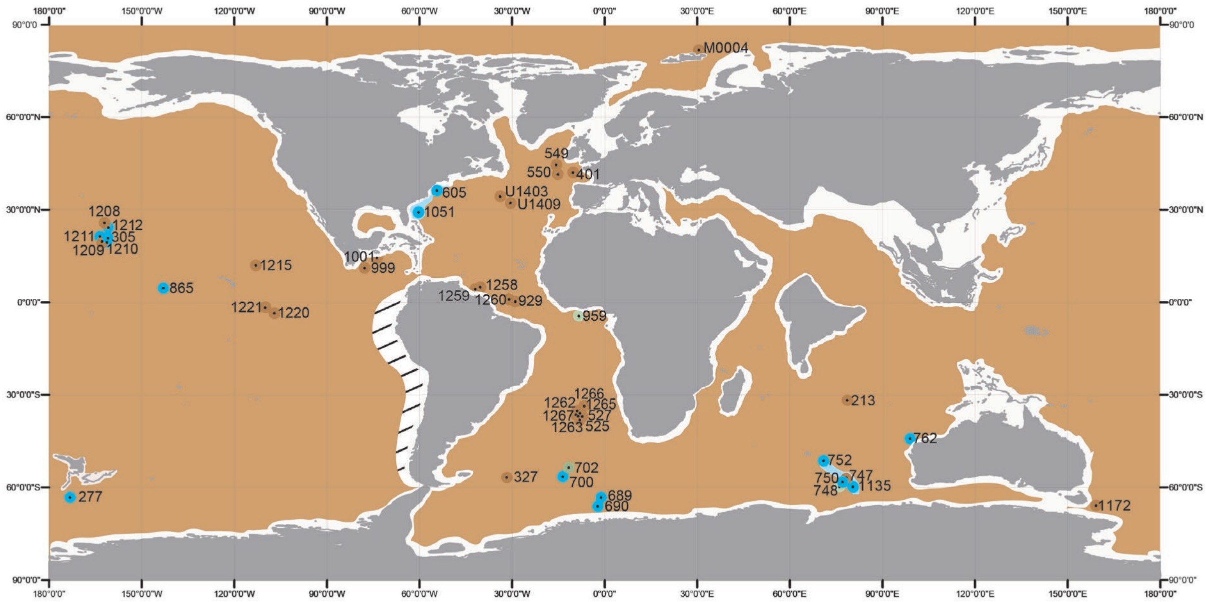

Figure 3. Ocean sediment distribution at the PETM (key as in Figure 1). Carbonate sediment distribution is greatly reduced globally. Clay is inferred at sites to reflect a lack of biogenic component, though sedimentation was probably negligible in areas such as the southwest Pacific (Rea et al., 2006). At the PETM, three sites record a dominant biosiliceous sediment component.

3.3 Upper Eocene sediment distribution

The ocean sediment core data indicate that the sediments deposited in the late Eocene were dominantly calcareous (Table 3). Approximately 100 sites show carbonate sediments distributed in all major ocean basins (Fig. 4), and a high concentration of calcareous-dominated sediment sites are located in the South Atlantic, Indian Ocean and the Gulf of Mexico. However, the calcareous sediments are not restricted to the low-latitude areas; sites in the Southern Ocean and North Atlantic also have carbonate sediments in the upper Eocene.

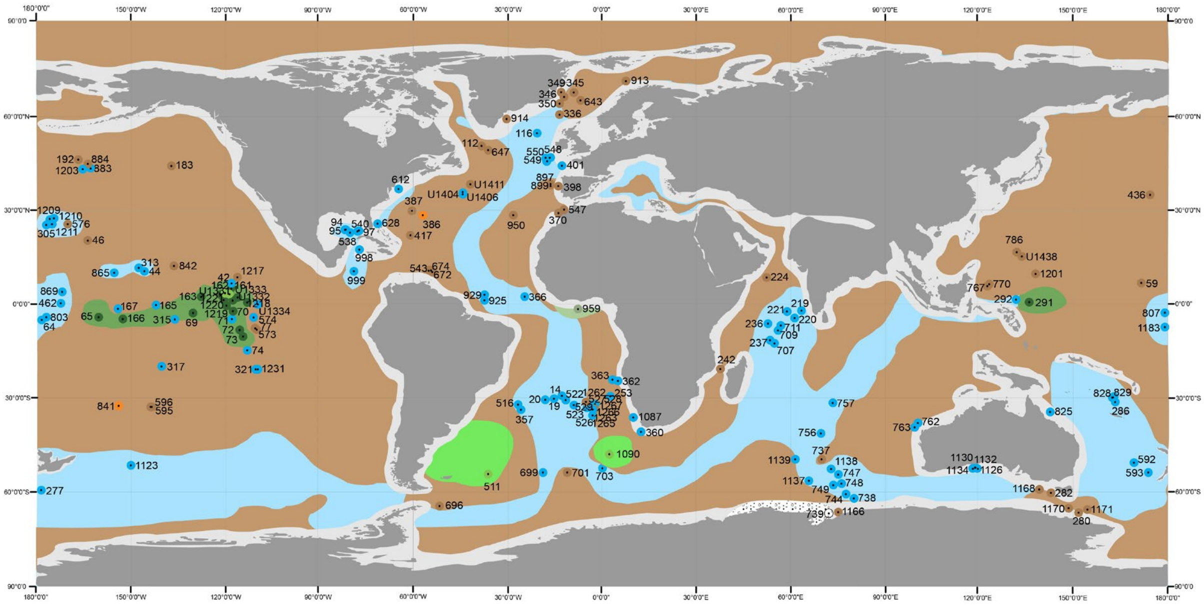

Figure 4. Ocean sediment distribution of the late Eocene (key as in Figure 1). Radiolarian oozes are found in the equatorial Pacific. Diatom oozes are located in the South Atlantic. Diamictite is documented in the late Eocene at Site 739. Paleobathymetry and the locations of ocean ridges were constrained using Muller et al. (2008) and He et al. (2019).

Siliceous sediments were recovered from ~15 late Eocene sites and consist mainly of radiolarian ooze with some diatom ooze. Radiolarian oozes are highly concentrated in the eastern equatorial Pacific (Fig. 5); only one site (Site 291) with radiolarian ooze is located in the western equatorial Pacific (Figs. 4, 7). Sites 511 and 1090, situated in southern part of the South Atlantic Ocean are diatom oozes. Porcellanite is recorded at Site 959, located in the eastern equatorial Atlantic.

Figure 5. Image of the >63 µm size fraction from upper Eocene Hole U1334A, 27X6, 43-45 cm (equatorial Pacific), showing the high abundance of radiolarian tests.

Siliciclastic sediments are generally found in sites that were situated near the continents, however, they are also found in the ocean basins. Turbidite-derived silty sand and clayey siltstone are recorded at Site 386, and volcanic sandstone at Site 841 (Fig. 4).

Clay was present in all the major oceans (Fig. 4), but mainly concentrated in the North Pacific and South Pacific oligotrophic gyres. Site 913, on the present day East Greenland margin, is the northernmost location in the EOT sediment distribution map and records clay sediments from the upper Eocene. Site 739, near Antarctica, has diatomite sediments of late Eocene age, but nearby, Site 1166 has only clay-dominated sediments.

3.4 Lower Oligocene sediment distribution

The lower Oligocene map (Fig. 6) shows a significant change from upper Eocene non-calcareous sediments including siliceous oozes, clay and siliciclastic sediment, to lower Oligocene calcareous sediments. The majority of late Eocene sites accumulating radiolarian sediments shifted to calcareous oozes in the early Oligocene. In the equatorial Pacific, most sites containing siliceous sediment transition from radiolarian-dominated sediment to nannofossil oozes as the major sediment component in the early Oligocene (Fig. 7). Only Sites 163 and 166 continued to see deposition of radiolarian dominated sediments. Apart from the significant change of radiolarian dominated sediments, some clay dominated sediments and siliciclastic sediments also changed to calcareous sediments through the EOT. Site 77 in the Pacific Ocean, Site 224 in Arabian sea and eastern Atlantic Ocean Site 547 showed a major component shift from clay to calcareous deposition at this time interval. Sites 1170 and 1171 in the Southern Ocean also record the change from siliciclastic to carbonate sediments during the EOT. Sites that recorded calcareous sedimentation during the late Eocene continued to see calcareous sedimentation across the EOT. The diatom oozes at Site 1090 and Site 511 in the South Atlantic Ocean and porcellanite at Site 959 in the eastern equatorial Atlantic persisted across the transition.

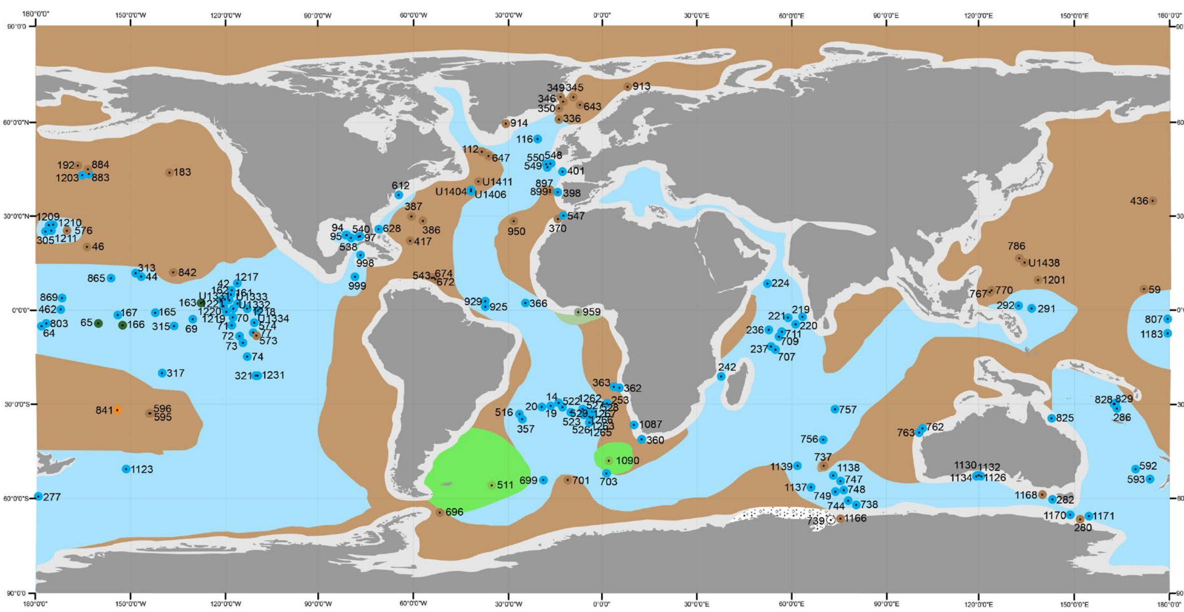

Figure 6. Ocean sediment distribution of the early Oligocene (key as in Figure 1). Diatom oozes are located in the South Atlantic. Carbonate ooze becomes the major modifier in the early Oligocene due to the fall in the CCD. Diamictite is documented at Site 739, with clayey mudstone with ice rafted debris recorded at Site 696. Paleobathymetry and the locations of ocean ridges were constrained using Muller et al. (2008) and He et al. (2019).

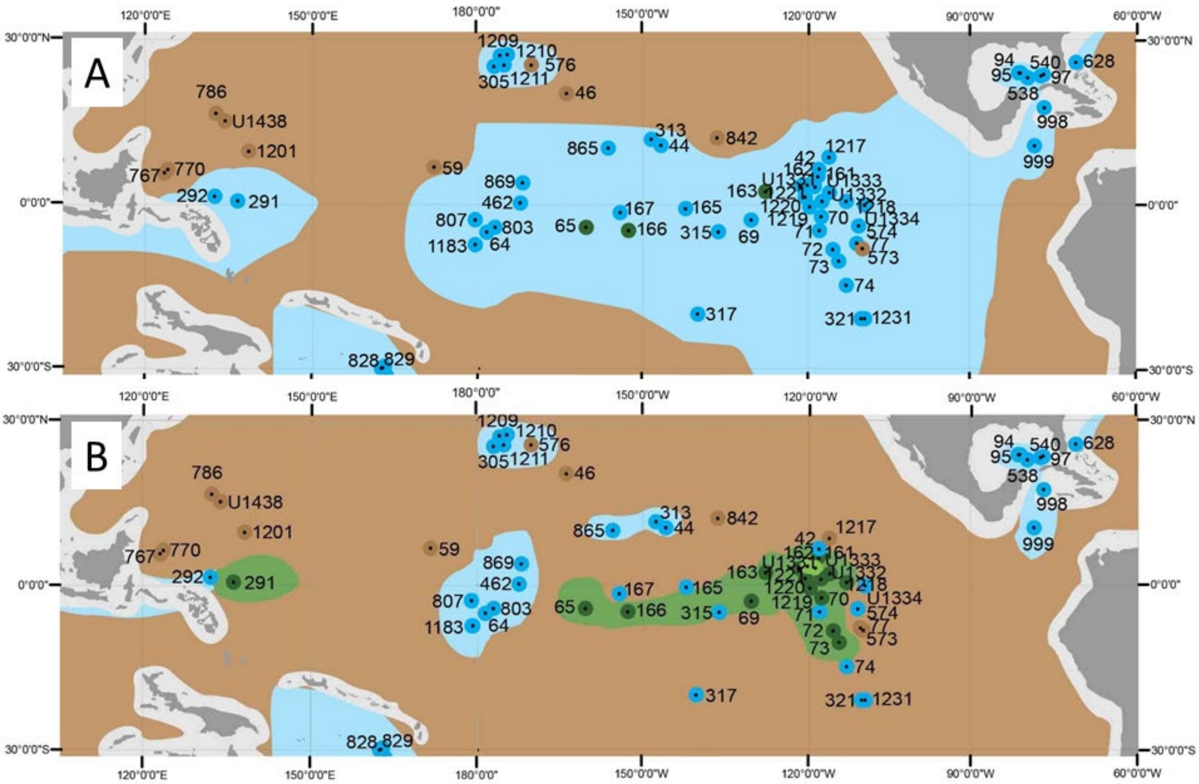

Figure 7. Close up of equatorial Pacific sediment distribution of the early Oligocene (A) and late Eocene (B), showing the shift in deposition from radiolarian to carbonate ooze (key as in Figure 1).

4. Discussion

4.1 Sediment distribution in the late Paleocene, and comparison to modern

Whilst it is well established that shoaling of the CCD occurred during the PETM resulted in a shoaling of the CCD, our compilation indicates the extent of carbonate distribution before and during the PETM. Comparative analysis of the maps produced herein (Figs. 2 and 3), both to one another and to those showing modern ocean sediment distributions (Fig. 1), demonstrates how key oceanic and climatic parameters are altered by this perturbation in Earth's climate state.

Upper Paleocene deep-sea sediments are dominated by carbonates and clay. The distribution of carbonate sediments for the upper Paleocene (Fig. 2) shows marked differences compared to that of the modern, particularly in the Southern Ocean. In the modern Southern Ocean, diatomaceous oozes represent the dominant sediment type (Fig. 1), with only minor and isolated regions of carbonate sediment deposition (Dutkiewicz et al., 2015). Conversely, the upper Paleocene sediment map (Fig. 2) shows broad regions of carbonate ooze around the Antarctic continent, reflecting differences in the late Paleocene ocean state compared to the modern. A primary control on carbonate sediment distribution in the open ocean is deposition above the CCD (van Andel, 1975). Paleobathymetry data for sites recording carbonate sediment deposition in the upper Paleocene show that all are located on relief features on the seafloor or along shallow continental margins. The broad region of nannofossil ooze to the west of Australia is inferred from sites located on-top or on-flank of the Kerguelen Plateau, and would have been significantly shallower than the surrounding seafloor (Frey et al., 2000). Similarly, the remainder of upper Paleocene carbonate sites sampled sediments deposited on submarine rises, ridges, plateaus, guyots and continental margins. The paucity of upper Paleocene siliceous sediments in the deep-sea realm has been taken to signify the confinement of biogenic siliceous sedimentation to the shelves, especially considering the extensive distribution of late Paleocene through early Eocene diatomite on the Eurasian Platform. On the other hand, however, the apparent scarcity of siliceous sediments in the deep-sea before the PETM could be due to non-preservation rather than non-deposition. For a discussion on the spatial and temporal trends in the distribution of the biosiliceous component in early Paleogene sediments of the Atlantic Ocean, albeit based on a different classification scheme, see Witkowski et al. (2020a).

4.2 Carbonate sediment distribution at the PETM

Sediment distribution at the PETM is dominated by clays (Fig. 3), reflecting wide-scale carbonate dissolution and CCD shoaling associated with significant carbon input to the atmosphere and oceans (Zachos et al., 2005). Diffusion of atmospheric CO_2 into the oceans resulted in lowered pH and a concomitant increase in the rate of $CaCO_3$ dissolution, temporarily ceasing carbonate deposition at many sites (Penman et al., 2014). The predominance of clay at the PETM also reflects a degree of 'carbonate burndown' (Griffith et al., 2015), wherein $CaCO_3$ in the upper ~10-40 cm of the pelagic sedimentary cover underwent dissolution as more acidic deep ocean water percolated down through seafloor sediments (Kelly et al., 2010). Though carbonate ooze persists at some sites at the PETM (Fig. 3), this is largely an artefact of the broad sediment classification used herein, which conceals partial dissolution observed at all PETM carbonate sites, such as Site 690 where wt% $CaCO_3$ decreased from >76 to ～61% (Bralower et al., 2014).

Comparison of Pacific Ocean (Shatsky Rise) and Atlantic Ocean (Walvis Ridge) sediment changes across the PETM reveals significant divergence in the dissolution response of each basin to C input. In the western Pacific, Shatsky Rise sites with paleodepths between 2,000 and 3,000 m maintain nannofossil ooze (Table 2) with $CaCO_3$ wt% of >75% (Colosimo et al., 2006). Conversely, Walvis Ridge sites with paleodepths in the range of 1,500-3,600 m have clay as the major lithology (Table 2) and contained virtually no carbonate at the PETM

(Zachos et al., 2005). The divergent dissolution responses of the two major ocean basins reflect more extensive CCD shoaling in the Atlantic, where the PETM CCD occupied depths of ~1,500 m, compared to ~3,000 m in the Pacific (Zeebe and Zachos, 2007; Panchuk et al., 2008). Indeed, Atlantic CCD shoaling was so extensive that it extended up onto the shelf (Self-Trail et al., 2017; Bralower et al., 2018). This suggests an Atlantic source of PETM carbon, either from North Atlantic Igneous Province volcanism (Saunders, 2016), extensive methane hydrate destabilization or a combination of both, though circulation change has also been proposed to explain the variance between the Atlantic and Pacific CCD shoal (Zeebe and Zachos, 2007; Zeebe et al., 2009).

There is an indication of meridional gradients in carbonate chemistry in the southern Atlantic. Comparison of Site 1263 (Walvis Ridge; 2,717 m water depth) and Site 690 (Weddell Sea; 2,914 m water depth) record markedly different dissolution responses to the PETM, despite their comparable paleodepths. The CCD shoaled by around 2,000 m at Site 1263, causing dissolution of $CaCO_3$ and a resultant clay layer with $CaCO_3$ wt% of <1% (Zachos et al., 2005); whilst the CCD remained below 2,000 m at Site 690 with nannofossil ooze recorded in both the late Paleocene and PETM (Figs. 2 and 3, Table 2). The suggested gradient in carbonate saturation from south to north is also evident in the comparatively expanded PETM section at Site 690, indicative of higher sediment input in the form of carbonate material and therefore less extensive dissolution at the PETM (Kelly et al., 2010). The presence of a latitudinal carbonate saturation gradient undermines the assertion that Atlantic meridional overturning temporarily reversed at the PETM (e.g., Bice and Maroatzke, 2002; Nunes and Norris, 2006). Had deep water formation switched from the Southern Ocean to the North Atlantic, waters with higher dissolved CO_2 (a result of longer exposure to respiring biota) would have bathed Site 690, whilst less corrosive waters would be expected at the more northerly Walvis Ridge.

4.3 Biosiliceous sediment distribution at the PETM

Penman (2016) suggested that increased weathering across the PETM would lead to enhanced silica availability and that porcellanite and chert are exceptionally common in the Eocene Atlantic Ocean (Penman et al., 2019). However, this is not reflected in our data set (Figs. 2 and 3). Chert is present at sites 702 and 748, with porcellanite at Site 959. Sites with poor recovery (which could be due to chert, e.g., sites 698, U1407) have not been included in our compilation, which most likely results in an underestimation of chert occurrences. While the low biosiliceous deposition may, to some extent, be an artefact of the classification scheme, we do not find extensive siliceous sedimentation as seen in the modern and late Eocene sediment maps (Figs. 1 and 4), and the major modifier is predominately carbonate or clay (Figs. 2 and 3). Our study does not prohibit the enhanced silica burial as suggested by Penman et al. (2019) but does show that even with enhanced weathering and increased Si input, siliceous ooze is not the major modifier in most PETM sites. Enhanced biosiliceous sedimentation does appear to be linked to PETM at Eurasian Platform sites, where extensive deposition of diatomite and diatom clays took place through much of the early Paleogene (e.g., Oreshkina, 2012; Oreshkina and Radionova, 2014).

Site 959, located in the eastern equatorial Atlantic records porcellanite in all four time slices from the late Paleocene (~56.5 Ma) to early Oligocene (~33.5 Ma) (Figs. 2, 3, 4 and 6). Sediments are also elevated in total organic carbon (Shipboard Scientific Party, 1996). As porcellanite is derived from recrystallization of biosiliceous opal-A to opal-CT, it suggests that there was a sustained source of nutrients to this region throughout the early Paleogene, leading to high biosiliceous deposition. Nutrients may have been derived from upwelling or terrestrial influx. Cramwinckel et al. (2018) proposed that upwelling occurred in the middle and late Eocene at Site 959, based on the presence of Protoperidiniaceae cysts. However, our work suggests that upwelling/nutrient influx started before the late Paleocene, and continued into the Oligocene.

In the modern ocean, biosiliceous sediments are a major constituent with diatomaceous ooze surrounding much of Antarctica (Dutkiewicz et al., 2015). One of the major findings of this paper is the documentation of the global paucity of biosiliceous sediments as the major modifier, compared to the modern ocean, despite both diatoms and radiolarians being ubiquitous in the early Paleogene (Witkowski et al., 2020a). There is no major turnover in radiolarians at the PETM, though Sanfilippo and Blome (2001) record a decrease in preservation and abundance. Does the absence of biosiliceous sedimentation as the major modifier, reflect a deficiency in biogenic silica production (e.g., a more diffuse nutrient regime), warm deep waters impacting biogenic silica preservation and burial, or a mixture of other mechanisms?

The availability of macronutrients (nitrate and phosphate) and micronutrients (iron) is a major control on the distribution and abundance of diatoms. The low meridonial gradient, and lack of vertical mixing would have left limiting nutrients locked in the subsurface (Moore et al., 2008). Productivity proxies for the late Paleocene are rare and controversial, with most studies concentrating on the potential role of export productivity in the early Eocene as a mechanism of CO_2 drawdown (e.g., Paytan et al., 2007). Fontorbe et al. (2016, 2020) showed that oceanic dissolved silica is depleted throughout the water column in the North Atlantic during the PETM (see also Witkowski et al., 2000b for revised age model). Moore et al. (2008) also documented that siliceous deposits of the Eocene are less common than modern, suggesting that silica input in the Eocene was lower. The deficiency of biogenic silica deposition around Antarctica at the PETM could, in part, be attributable to the sluggish circulation and inhibition of nutrient-rich upwelling across this interval (Heinze and Ilyina, 2015), and, on a more regional level, by the absence of a strong circumpolar current (Hill et al., 2013; Katz et al., 2011). Changes occurred soon after the PETM with cherts and siliceous microfossils preserved in the South Atlantic in the Eocene (Witkowski et al., 2020a).

Equatorial divergence brings nutrient-rich waters to the surface where they are readily utilised by plankton. At the equator, the apparent absence of biosiliceous sediments can also be linked to reduced upwelling and lack of nutrient supply associated with comparatively weaker trade winds resulting from diminished latitudinal temperature gradients (Moore et al., 2002, 2004; Lyle et al., 2008; Heinze and Ilyina, 2015). This effect would have been further compounded by warming across the PETM (Winguth et al., 2012).

Diatom abundance and diversification through the Cenozoic can also explain the absence of biogenic silica-dominated sites across the PETM. It has been shown that, over geological timescales, diatom species diversity correlates with net biosiliceous sediment export productivity (Lazarus, 2011). Though species turnover increased in response to the PETM (Oreshkina, 2012), enhanced diversity at this time was largely the result of greater endemism, particularly at high latitudes and in epicontinental seas (Lazarus et al., 2014; Barron et al., 2015). In the open oceans, diminished latitudinal temperature gradients would have suppressed oceanic heterogeneity and therefore diatom species proliferation, precluding large-scale biogenic silica deposition (Lazarus et al., 2014). Sims et al. (2006) proposed that diatoms transferred to the open ocean from the shelf through the Cenozoic. This view reconciles the rich fossil record from early Paleogene onshore sites, especially on the Eurasian Platform (Barron et al., 2015), with the scarcity of early Cenozoic diatoms in the deep-sea (Lazarus et al., 2014; Renaudie, 2016).

The scarcity of biosiliceous sediments in the early Paleogene may be attributed to dissolution. In the modern ocean, diatomaceous sediment deposition correlates with areas of low SSTs (<6°C) (Dutkiewicz et al., 2015). The solubility of biogenic silica is positively correlated with ocean temperature (Kamatani, 1982), and thus would more rapidly dissolve in the warmer ocean waters of the early Paleogene. Moreover, optimal diatom growth occurs where SSTs are significantly lower than those inferred for any sites during the late Paleocene/early Eocene (Neori and Holm-Hansen, 1982; Hollis et al., 2019). Further to this, recent studies have shown that diatom silicification is inhibited with high CO_2 and thus lower pH (Petrou et al., 2019). The environmental conditions of the early Paleogene would have therefore influenced the distribution and preservation of siliceous organisms in the deep-sea realm.

Finally, during diagenesis, biosilica may be mobilized and redeposited as chert nodules and beds, transferring the siliceous sediments to different horizons. Witkowski et al. (2020a) show that the geographic distribution of lower Paleocene through upper Eocene chert and porcellanite in the Atlantic Ocean closely matches that of the biogenic siliceous sediments, which suggests that the picture of biogenic silica deposition in the early Cenozoic oceans is strongly biased due to diagenetic alteration.

4.4 Sedimentary changes across the Eocene-Oligocene transition

Global climate change across the EOT affects the sediment deposition pattern and is mainly characterized by the shift in the CCD. Calcareous sediments are dominant in both late Eocene and early Oligocene, however, the distribution in the early Oligocene is more extensive due to the change from non-carbonate to carbonate deposition. The late Eocene CCD was relatively shallow at approximately 3,300 m and varies between ocean basins (van Andel, 1975, Rea and Lyle, 2005; Pälike et al., 2012). The Pacific Ocean experienced the most dramatic CCD deepening (>1,000 m) (van Andel, 1975, Heath et al., 1977; Lyle et al., 2002; Rea and Lyle, 2005; Pälike et al., 2012) across the EOT.

4.4.1 Carbonate compensation depth

A prominent feature of the upper Eocene sediment map is the occurrence of radiolarian oozes in the eastern equatorial Pacific, which indicate the upwelling and advection of silicic acid and nutrients to surface waters in equatorial regions (Figs. 4 and 7b). This feature is referred to as the 'equatorial tongue of high productivity' (Moore et al., 2004). The distribution of siliceous sedimentation in the equatorial Pacific Ocean suggests that upwelling was initiated in the Eocene as latitudinal gradients increased. Radiolarian accumulation rates in the eastern equatorial Pacific decreased at the EOT (Moore et al., 2014), related to changes in ocean circulation (e.g., the source of the upwelled water at the equatorial divergence) impacting the nutrient concentration of advected subsurface waters (Funakawa et al., 2006; Moore et al., 2014).

The signal of deepening of the CCD across the EOT is shown in the sediment distribution changes in most sites in the equatorial Pacific (ODP Leg 198, 199, IODP Leg 320) with the disappearance of siliceous sediments (Fig. 7). Radiolarian ooze in the eastern equatorial Pacific is surrounded by isolated areas of carbonate ooze, on the topographic highs, above the CCD. For example, Site 167 was drilled on the Magellan Rise, and Site 317 is located on the Manihiki Plateau, at water depths of 3,200 m and 2,600 m, respectively. The deepening of the CCD at the EOT allowed carbonate to be deposited at greater depth and caused a major composition change from radiolarian-dominated to calcareous-dominated sediments in the early Oligocene. Consequently, the distribution of siliceous sediments decreased. The early Oligocene equatorial Pacific sediments still contain a high abundance of siliceous organisms, however, silica is no longer the major modifier. Indeed, diatom deposition in the equatorial Pacific actually increases across the EOT (Moore et al., 2014), but the signal is masked by enhanced carbonate deposition.

Apart from the CCD drop at the EOT, which changed the major modifier from radiolarian to carbonate ooze in the equatorial Pacific (Fig. 7), the disappearance of radiolarian oozes and decrease in radiolarian accumulation rates could be in part due to radiolarian faunal turnover related to the ocean cooling (Funakawa et al., 2006). Many species of radiolarians became extinct in a series of events during the middle and late Eocene and the EOT (Kamikuri and Wade, 2012; Moore and Kamikuri, 2012).

Evidence of CCD deepening in not restricted to the equatorial Pacific Ocean. In the Atlantic and Indian oceans, the CCD also shows evidence of decline, but less severe than the Pacific (van Andel, 1975, Rea and Lyle, 2005 and references therein). The sedimentary change across the EOT in the Atlantic and Indian Ocean is relatively minor, as most sites are persistently located above the CCD through the transition. In the Atlantic (e.g., sites 1262 and 1267) and Indian oceans (sites 224 and 242) there is a change in sedimentation from non-carbonate to carbonate-dominated across the EOT. Changes from non-carbonate to carbonate dominated deposition is recorded at sites 282, 1170 and 1171 in the Tasman Sea. Our depositional maps confirm that the CCD deepening occurred on a global scale (van Andel, 1975, Peterson et al., 1992; Rea and Lyle, 2005). Some adjacent sites indicate no change owing to a greater paleodepth which was deeper than the CCD.

The distribution of clay-dominated sediments during the EOT (as today) is generally dependent on ocean conditions that do not favour other types of sediment deposition, i.e., areas which are below the CCD and low productivity. Clay distribution at the EOT and in the modern ocean show a comparable distribution, though it is larger in the upper Eocene sediment map due to the shallower CCD, especially in the Atlantic Ocean.

4.4.2 South Atlantic diatom ooze

In the late Eocene and early Oligocene, the South Atlantic becomes an area for biogenic silica burial (Renaudie, 2016), with diatom-dominated sediments found at sites 1090 and 511 (Figs. 4 and 6). Our sedimentary maps indicate that the conditions changed from the early

Paleogene (Figs. 2 and 3) to the EOT (Figs. 4 and 6) to be more favourable to enhanced biosiliceous deposition in the South Atlantic (Fig. 3 and 4).

Diatom deposition is generally considered to be an indicator of high surface water productivity (phosphorous, nitrogen, silica) (Barron and Baldauf, 1989), though Dutkiewicz et al. (2015) have recently questioned this.The presence of diatom oozes does not solely reflect diatom productivity as measured by opal accumulation rates, and sedimentation rates have a significant effect on diatom preservation. It has previously been suggested (e.g., Renaudie, 2016), that enhanced weathering would have increased diatom deposition, due to higher silica availability. However, changes in ocean circulation likely drove divergence and wind driven upwelling in the South Atlantic, redistributing nutrient supplies from the subsurface to the surface ocean, particularly silica, nitrate and phosphate and allowing the development of siliceous oozes. The diatomaceous sediments potentially represent greater vertical mixing and intensified oceanic circulation (Miller et al., 2009; Houben et al., 2019b; Witkowski et al., in prep.), and the onset of an upwelling front (Plancq et al., 2014). A study from Site 1090 shows the occurrence of 'opal pulse' between late Eocene and earliest Oligocene which records the development of upwelling cells along topographic highs (Diekmann et al., 2004).

Stickley et al. (2004) suggested that biogenic silica deposition began around 45 Ma along the Antarctic margin, and Egan et al. (2013) indicated through silicon isotope ($\delta^{30}Si$) measurements, increased utilization of silicic acid occurring from the late Eocene. Antarctic weathering would have enhanced terrestrial-sourced micronutrients, i.e. iron, and relaxed iron limitation, allowing diatoms to thrive. Enhanced diatom abundance in the South Atlantic may be a potential mechanism for atmospheric CO_2 drawdown in the middle and late Eocene through an increased biological pump (Rabosky and Sorhannus, 2009; Salamy and Zachos, 1999; Scher and Martin, 2006; Egan et al., 2013). New views on the relationship between climate and terrestrial silicate weathering are emerging (see Caves et al. 2016), and it remains to be verified how siliceous plankton production may have responded to these new scenarios.

The distribution of diatom ooze does not significantly change across the EOT (Figs. 4 and 6), despite several studies indicating increased productivity in high southern latitudes (e.g. Site 744 and Site 689) (Diester-Haass, 1995; Diester-Haass et al., 1996; Salamy and Zachos, 1999; Latimer and Filippelli, 2002; Diester-Haass and Zahn, 2001; Diekmann et al., 2004; Anderson and Delaney, 2005; Plancq et al., 2014). There is evidence of increased abundance of diatoms (e.g., Site 744, Salamy and Zachos, 1999), however, carbonate remains the major modifier. We do not see the enhancement in productivity reflected in biosiliceous sediment deposition. Sediments close to Antarctica in the early Oligocene (e.g., Kerguelen Plateau and Tasman Sea) are carbonate, not siliceous oozes.

Surface water circulation patterns were altered by tectonic evolution and the opening and closing of gateways. The opening of the Drake Passage and the initiation of the Antarctic Circumpolar Current (ACC) is controversial, with estimates ranging from the middle Eocene to late Oligocene (Scher and Martin, 2006; Pfuhl and McCave, 2005; Katz et al., 2011; Scher et al., 2015). Recent modelling studies have suggested that productivity changes in response to the Drake Passage opening would have varied spatially (Ladant et al., 2018), with diatoms predominating at high latitudes. The sediment distribution in the late Eocene and early Oligocene does not change and thus does not support that the Drake Passage opened, or that the proto-ACC was initiated across the Eocene/Oligocene boundary.

We do not see any change or expansion biosiliceous depositional patterns across the EOT, indicating that the mechanisms to allow enhanced diatom deposition in the South Atlantic were in place before the end of the Eocene. The small number of early Oligocene diatomaceous dominated sites may also be an artefact of the distribution of ocean drilling sites. Of course, carbon export can increase without a change in biosiliceous sediment distribution, and recent modelling investigations by Ladant et al. (2018) indicate an increase in export production in the South Atlantic whilst diatom primary production decreases. The remineralization of organic matter through the water column is temperature dependent (John et al., 2013; Boscolo-Galazzo et al., in review), thus providing a mechanism to resolve the conflict here between sediment and productivity records.

The sediment distribution pattern of diatom-dominated sediments during the EOT is markedly different from modern oceans (Figs. 1, 4 and 6). Diatom oozes are not abundant at the EOT, and are only found in the South Atlantic (Figs. 4 and 6). Sites 1090 and 511 were located 47ºS and 54ºS, respectively, at the EOT (Table 3), very different to the current area of diatomaceous sediment accumulation in the modern ocean, where diatom-dominated sediments are highly concentrated in the circum-Antarctic belt (Dutkiewicz et al., 2015). At higher latitudes (>55ºS), deposition at the EOT is predominately carbonate e.g., Site 277, 738, 744, 748, 749, 1137, 1170, 1171 with a few clay dominated sites. We do not see find the extensive diatom oozes that are seen in the modern ocean (Fig. 1). Increased global cooling during the Eocene developed the strong differentiation between the high and low latitudes which invigorated oceanic circulation and enhanced biosiliceous sedimentation in the South Atlantic (Baldauf and Barron, 1990; Miller et al., 2009). Progressive climatic deterioration in the Neogene increased the thermal gradient, resulting in the geographically restricted upwelling regions observed today and development of the opal belt around Antarctica (Baldauf and Barron, 1990; Cortese et al., 2004).

4.6 Glaciomarine deposition at the EOT

The most significant event of the EOT is the appearance of a continental-scale ice sheet on Antarctica and glaciomarine sediments are the most direct evidence. Some cores indicate the onset of glaciation on Antarctica during the EOT, through the presence of ice-rafted debris

(IRD) and glacial diamictites (Wise et al., 1991, 1992; Breza and Wise, 1992; Zachos et al., 1992; Ehrmann and Mackensen, 1992; Ivany et al., 2006; Scher et al., 2014). Sites 696, 738, 742, 744 and 748 contain IRD but as a minor component (Carter et al., 2017; Barron et al., 1991); Site 742 is not complete and thus has been excluded from our compilation. In the ocean sediment distribution maps of the late Eocene and early Oligocene (Figs. 4 and 6), diamictite occurs near the Antarctic continent at Site 739, located in Prydz Bay, East Antarctica, implying that glaciers in this area reached sea level during late Eocene. In the earliest Oligocene, despite widespread evidence of an Antarctic ice sheet, we do not find glaciomarine sediments as the major modifier at any other DSDP, ODP or IODP site.

5. Conclusions

We compiled ocean sedimentary maps of the late Paleocene, PETM, late Eocene and early Oligocene, based on sediment lithology records from DSDP, ODP and IODP, to document the sedimentary changes across two of the most significant climate events in the Cenozoic. Our tables provide a catalogue of all existing ocean drilling sites covering these intervals drilled to date. In mapping sediment distribution and composition, we provide a graphic synthesis of the extent of climatic change as recorded in the ocean sediment cores. Sedimentary changes across the PETM, chiefly the emergence of clays as the major sediment type and the dissolution of carbonates are evidence of widespread shoaling of the CCD. Our study also illustrates how the deposition of siliceous sediments altered through the early Paleogene. During the latest Paleocene and PETM, biogenic silica deposition was low in comparison to the modern. Diminished biosiliceous deposition is explained in the context of a more diffuse upwelling regime which persisted across the interval of study, coupled with reduced diatom abundance and dissolution of silica in the warm early Paleogene oceans. For the late Paleocene, carbonate sediments are shown to have been pervasive, extending to far southerly latitudes and this is commensurate with the warm, oligotrophic ocean state. Across the EOT, the CCD dramatically deepened, manifesting in a shift at many locations, from non-calcareous to calcareous dominated sediments. The prominent feature of the late Eocene map is the tongue of radiolarian oozes in the eastern equatorial Pacific which relate to shallower CCD and equatorial divergence. Our depositional maps confirm the global scale deepening of the CCD across the EOT. In the Eocene South Atlantic, diatom dominated sediments develop but the pattern differs from the modern distribution, with carbonate rich sediments bordering Antarctica, unlike the glacial and siliceous rich sediments seen today.

The maps of sediment data help to indicate and visualise past ocean conditions and contribute to the understanding of biogeochemical cycles in the ocean in response to the climate change. Undoubtedly, as more ocean drilling data becomes available, more accurate mapping of the seafloor sediment can be achieved with improved resolution and coverage.

Acknowledgements

We are grateful to two anonymous reviews, whose comments greatly improved the manuscript and sediment maps. We thank Jerry Dickens for comments on earlier versions of the maps, and Anna Joy Drury and Kate Hendry for discussion. Sediment information used in this study was compiled from the International Ocean Discovery Program (IODP) and its predecessors. IODP is sponsored by the U.S. National Science Foundation and participating countries. Funding: BW was supported by UK Natural Environment Research Council (NERC) [reference number NE/G014817]. Support for JW was provided by the Polish National Science Centre [grant number 2016/21/B/ST10/02937].

References

Alegret, L., Ortiz, S. and Molina, E., 2009, Extinction and recovery of benthic foraminifera across the Paleocene–Eocene Thermal Maximum at the Alamedilla section (Southern Spain): Palaeogeography, Palaeoclimatology, Palaeoecology, 279, 186-200.

Anderson, L.D. and Delaney, M.L., 2005. Middle Eocene to early Oligocene paleoceanography from Agulhas Ridge, Southern Ocean (Ocean Drilling Program Leg 177, Site 1090). Paleoceanography, 20(1), PA1013

Baldauf, J.G., and Barron, J.A., 1990. Evolution of biosiliceous sedimentation patterns for the Eocene through Quaternary: Paleoceanographic response to polar cooling, in Thiede J. and Beil U. eds., Geologic History of the Polar Oceans: Arctic versus Antarctic. Kluwer Academic Publication Group, Dordrecht, Holland, 575-608.

Barron, E.J. and Whitman, J.M. 1981. Oceanic sediments in space and time. in Emiliani, C., ed., The Sea, Volume 7: New York, Wiley Interscience, 689-733.

Barron, J.A. and Baldauf, J.G., 1989. Tertiary cooling steps and paleoproductivity as reflected by diatoms and biosiliceous sediments. In: Berger, W.H., Smetacek, V.S., and Wefer, G. (eds.) Productivity of the Ocean: Present and Past. John Wiley and Sons Ltd: 341-354.

Barron, J. A., Baldauf, J. G., Barrera, E., Caulet, J.-P., Huber, B. T.,Keating, B. H., Lazarus, D., Sakai, H., Thierstein, H. R., andWei, W., 1991. Biochronologic and magnetochronologic synthesisof Leg 119 sediments from the Kerguelen Plateau and Prydz Bay,Antarctica. In Barron, J., Larsen, B., et al., Proc. ODP, Sci.Results, 119: College Station, TX (Ocean Drilling Program), 813-848.

Barron, J.A., Stickley, C.E., and Bukry, D., 2015, Paleoceanographic, and paleoclimatic constraints on the global Eocene diatom and silicoflagellate record. Palaeogeography, Palaeoclimatology, Palaeoecology, 422, 85-100. doi:10.1016/j.palaeo.2015.01.015

Berger, W.H., Adelseck Jr. C.G., and Mayer L.A., 1976, Distribution of carbonate in surface sediments of the Pacific Ocean. J. Geophys Res 81,15, 2617-2627.

Bice, K.L. and Maroatzke J., 2002, Could changing ocean circulation have destabilized methane hydrate at the Paleocene/Eocene boundary? Paleoceanography, 17, doi:10.1029/2001PA000678

Boscolo-Galazzo, F., Crichton, K.A., Ridgwell, A., Mawbey, E.M., Wade, B.S. and Pearson, P.N. in review. Temperature controls carbon cycling and biological evolution in the ocean twilight zone. Science.

Bowen, G.J., Maibauer, B.J., Kraus, M.J., Röhl, U. and Westerhold, T., 2015, Two massive, rapid releases of carbon during the onset of the Paleocene–Eocene thermal maximum: Nature Geoscience, 8, 44-47, doi:10.1038/ngeo2316

Boyden, J. A., Müller, R. D., Gurnis, M., Torsvik, T. H., Clark, J. A., Turner, M., Ivey-Law, H.,Watson, R. J., and Cannon, J. S., 2011. Next-generation plate-tectonic reconstructions using GPlates, in: Geoinformatics: cyberinfrastructure for the solid earth sciences, edited by: Keller, G. and Baru, C., Cambridge University Press, Cambridge, UK, 95–114.

Bralower, T., Meissner, K.J., Alexander, K. and Thomas, D.J., 2014, The dynamics of global change at the Paleocene-Eocene thermal maximum: A data-model comparison: Geochemistry, Geophysics, Geosystems, 15, 3830-3848, doi: 10.1002/2014GC005474

Bralower, T.J., Kump, L.R., Self-Trail, J.M., Robinson, M.M., Lyons, S., Babila, T., Ballaron, E., Freeman, K.H., Hajek, E., Rush, W., Zachos, J.C., 2018, Evidence for shelf acidification during the onset of the Paleocene-Eocene Thermal Maximum. Paleoceanography and Paleoclimatology, 33, 1408-1426. https.//doi.org/10.1029/2018PA003382.Breza, J.R. and Wise, S.W. 1992. Lower Oligocene ice-rafted debris on the Kerguelen Plateau: evidence for East Antarctic

Continental Glaciation. In: Wise, S.W., Schlich, R.; et al. (eds.), Proceedings of the Ocean Drilling Program, Scientific Results, College Station, TX (Ocean Drilling Program), 120, 161-178.

Calvert. S.E. 1974, Deposition and diagenesis of silica in marine sediments. Spec. Pub. Im. Assn. Sediment. 1: 273-299.

Carter, A., Riley, T. R., Hillenbrand, C.-D., and Rittner, M., 2017. Widespread Antarctic glaciation during the Late Eocene. Earth and Planetary Science Letters, 458, 49-57.

Caves, J.K., Jost, A.B., Lau, K.V., and Maher, K., 2016, Cenozoic carbon cycle imbalances and a variable weathering feedback. Earth and Planetary Science Letters, 450, 152-163.

Chester, R. and Jickells, T.D., 2012, Marine Geochemistry (Third edition). Wiley-Blackwell, Oxford, UK. 411 pp.

Colosimo, A., Bralower, T.J., and Zachos, J.C., 2006, Evidence for lysocline shoaling at the Paleocene/Eocene Thermal Maximum on Shatsky Rise, Northwest Pacific, *in* Bralower, T.J., et al., Proceedings of the Ocean Drilling Program, Scientific results, Volume 198: College Station, Texas, Ocean Drilling Program, p. 1–36, doi: 10.2973/odp.proc.sr.198.112.2006.

Cortese, G., Gersonde, R. Hillenbrand, C. D. and Kuhn, G. 2004. Opal sedimentation shifts in the World Ocean over the last 15 Myr, Earth Planet. Sci. Lett., 224, 509–527.

Coxall, H.K., Wilson, P.A., Pälike, H., Lear, C.H., and Backman, J. 2005. Rapid stepwise onset of Antarctic glaciation and deeper calcite compensation in the Pacific Ocean. Nature, 433 (7021), 53-57.

Cramwinckel, M.J., Huber, M., Kocken, I.J. Agnini, C., Bijl, P.K., Bohaty, S.M., Frieling, J., Goldner, A., Hilgen, F.J., Kip, E.L., Peterse, F., van der Ploeg, R., Schouten, S. and Sluijs, A., 2018. Synchronous tropical and polar temperature evolution in the Eocene. Nature 559, 382–386.

Davies, T.A. and Gorsline, D.S. 1976. The geochemistry of deep-sea sediments. In: Riley, J.P. and Chester, R. eds., Chemical oceanography, Volume 5: London, Academic Press, 1-80.

DeMaster, D.J., 2014, The diagenesis of biogenic silica: Chemical transformations occurring in the water column, seabed, and crust: In: Treatise on Geochemistry, 9: 103-111.

Dickens, G.R., 2011, Down the Rabbit Hole: toward appropriate discussion of methane release from gas hydrate systems during the Paleocene-Eocene thermal maximum and other past hyperthermal events: Climate of the Past, 7, 831-846, doi:10.5194/cp-7-831-2011.

Dickens, G.R., O'Neil, D., Rea, D.K., and Owen, R.M., 1995, Dissociation of oceanic methane hydrate as a cause of the carbon isotope excursion at the end of the Paleocene: Paleoceanography, 10, 965–971, doi:10.1029/95PA02087.

Diekmann, B., Kuhn, G., Gersonde, R., Mackensen, A., 2004. Middle Eocene to early Miocene environmental changes in the sub-Antarctic Southern Ocean: evidence from biogenic and terrigenous depositional patterns at ODP Site 1090. Global and Planetary Change, 40, 295-313.

Diester-Haass, L. 1995. Middle Eocene to early Oligocene paleoceanography of the Antarctic Ocean (Muad Rise, ODP Leg 113, Site 689): change from a low to a high productivity ocean. Paleogeogr. Paleoclimat. Paleoecol. 113, 311-334.

Diester-Haass, L., and Zahn, R., 2001. Paleoproductivity increase at the Eocene–Oligocene climatic transition: ODP/DSDP sites 763 and 592. Paleogeogr. Paleoclimat. Paleoecol. 172, 153-170.

Diester-Haass, L., Robert, C. and Chamley, H., 1996. The Eocene-Oligocene preglacial-glacial transition in the Atlantic sector of the Southern Ocean (ODP site 690). Marine Geology, 131, 123-149.

Dunkley Jones, T., Bown, P.R., Pearson, P.N., Wade, B.S., Coxall, H.K., and Lear, C.H. 2008. Major shifts in calcareous phytoplankton assemblages through the Eocene-Oligocene transition of Tanzania and their implications for low-latitude primary production. Paleoceanography, 23, PA4204, doi:10.1029/2008PA001640.

Dunkley Jones, T., Lunt, D.J., Schmidt, D.N., Ridgewell, A., Sluijs, A., Valdes, P.J. and Maslin, M., 2013, Climate model and proxy data constraints on ocean warming across the Paleocene–Eocene Thermal Maximum: Earth-Science Reviews, 125, 123-145, doi: 10.1016/j.earscirev.2013.07.004

Dutkiewicz, A., Müller, R. D., O'Callaghan, S., and Jónasson, H. 2015. Census of seafloor sediments in the world's ocean. Geology, 43(9), 795-798. doi:10.1130/G36883.1

Egan, K.E., Rickaby, R.E.M., Hendry, K.R. and Halliday, A.N., 2013, Opening the gateways for diatoms primes Earth for Antarctic glaciation: Earth and Planetary Science Letters, v. 375, p.34-43, doi:10.1016/j.epsl.2013.04.030

Ehrmann, W. U. and Mackensen, A. 1992. Sedimentological evidence for the formation of an East Antarctic ice sheet in Eocene/Oligocene time. Palaeogeography, Palaeoclimatology, Palaeoecology, 93(1), 85-112.

Farley, K.A. and Eltgroth, S.F. 2003. An alternative age model for the Paleocene-Eocene thermal maximum using extraterrestrial 3He. Earth and Planetary Science Letters, 208, 135-148.

Firth, J.V., Eldrett, J.S., Harding, I.C., Coxall, H.K., and Wade, B.S., 2013. Integrated biomagnetochronology for the Palaeogene of ODP Hole 647A: implications for correlating palaeoceanographic events from high to low latitudes. In: Jovane, L., Herrero-Bervera, E., Hinnov, L. A. and Housen, B. A. (Eds.) Magnetic Methods and the Timing of Geological Processes. Geological Society, London, Special Publications, 373, 29-78. http://dx.doi.org/10.1144/SP373.9

Fontorbe, G., Frings, P.J., De La Rocha, C.L., Hendry, K.R., and Conley, D.J., 2016, A silicon depleted North Atlantic since the Palaeogene:Evidence from sponge and radiolarian silicon isotopes, Earth Planet. Sci. Lett., 453, 67–77.

Fontorbe, G., Frings, P. J., De La Rocha, C. L., Hendry, K. R., & Conley, D. J., 2020. Constraints on Earth system functioning at the Paleocene-Eocene thermal maximum from the marine silicon cycle. Paleoceanography and Paleoclimatology, 35, e2020PA003873. https://doi.org/10.1029/2020PA003873

Frey, F.A., Coffin, M.F. and Wallace, P.J., 2000, Origin and evolution of a submarine large igneous province: the Kerguelen Plateau and Broken Ridge, southern Indian Ocean: Earth and Planetary Science Letters, 176, 73-89, doi:10.1016/S0012-821X(99)00315-5

Frieling, J., Svensen, H.H., Planke, S., Cramwinckel, M.J., Selnes, H., Sluijs, A., 2016. Thermogenic methane release as a cause for the long duration of the PETM. Proc. Natl. Acad. Sci. 113, 12059–12064. doi:10.1073/pnas.1603348113

Frieling, J., Gebhardt, H., Huber, M., Adekeye, O.A., Akande, S.O., Reichart, G.-J., Middelburg, J.J., Schouten, S., Sluijs, A., 2017. Extreme warmth and heat-stressed plankton in the tropics during the Paleocene-Eocene Thermal Maximum. Sci. Adv. 3, e1600891. doi:10.1126/sciadv.1600891

Frieling, J., Peterse, F., Lunt, D. J., Bohaty, S. M., Sinninghe Damsté, J. S., Reichart, G.-J., and Sluijs, A., 2019.Widespread warming before and elevated barium burial during the Paleocene-Eocene Thermal Maximum: Evidence for methane hydrate release? Paleoceanography and Paleoclimatology, 34, 546–566. https://doi.org/10.1029/2018PA003425

Funakawa, S., Nishi, H., Moore, T.C., Nigrini, C.A., 2006. Radiolarian faunal turnover and paleoceanographic change around Eocene/Oligocene boundary in the central equatorial

Pacific, ODP Leg 199, Holes 1218A, 1219A, and 1220A. Palaeogeograhy. Palaeoclimatology. Palaeoecology, 230, 183-203.

Garcia, H. E., Locarnini, R. A. Boyer, T. P. Antonov, J. I. Zweng, M. M. Baranova, O. K.and Johnson, D.R., 2010, World Ocean Atlas 2009, Volume 4: Nutrients (phosphate, nitrate, and silicate), in NOAA Atlas NESDIS 71, edited by S. Levitus, p. 398, U.S. Government Printing Office, Washington, D.C.

Griffith, E.M., Fantle, M.S., Eisenhauer, A., Paytan, A. and Bullen, T.D., 2015. Effects of ocean acidification on the marine calcium isotope record at the Paleocene–Eocene Thermal Maximum: Earth and Planetary Science Letters, 419, 81-92, doi: 10.1016/j.epsl.2015.03.010

He, Z., Zhang, Z., Guo, Z. 2019. Reconstructing early Eocene (~55 Ma) paleogeographic boundary conditions for use in paleoclimate modelling. Science China Earth Sciences, 62: 1416–1427, https://doi.org/10.1007/s11430-019-9366

Heath, G.R., Moore, T.C. Jr., and van Andel, T.H. 1977. Carbonate accumulation and dissolution in the equatorial Pacific during the past 45 million years. In Andersen, N.R., and Malahoff, A. (Eds.). The Fate of Fossil Fuel CO2 in the Oceans. New York (Plenum), 627-639.

Heinze, M. and Ilyina, T., 2015, Ocean biogeochemistry in the warm climate of the late Paleocene: Climate of the Past, 11, 63-79.

Hill, D.J., Haywood, A.M., Valdes, P.J., Francis, J.E., Lunt, D.J., Wade, B.S. and Bowman, V.C., 2013. Paleogeographic controls on the onset of the Antarctic Circumpolar Current. Geophysical Research Letters, 40: 5199–5204.

Hollis, C.J., Hines, B.R., Littler, K., Villasante-Marcos, V., Kulhanek, D.K., Strong, C.P., Zachos, J.C., Eggins, S.M. 2015 The Paleocene-Eocene Thermal Maximum at DSDP

Site 277, Campbell Plateau, southern Pacific Ocean. Climate of the past, 11(7): 1009-1025, doi: 10.5194/cp-11-1009-2015

Hollis, C. J., Dunkley Jones, T., Anagnostou, E., Bijl, P. K., Cramwinckel, M. J., Cui, Y., Dickens, G. R., Edgar, K. M., Eley, Y., Evans, D., Foster, G. L., Frieling, J., Inglis, G. N., Kennedy, E. M., Kozdon, R., Lauretano, V., Lear, C. H., Littler, K., Meckler, N., Naafs, B. D. A., Pälike, H., Pancost, R. D., Pearson, P., Royer, D. L., Salzmann, U., Schubert, B., Seebeck, H., Sluijs, A., Speijer, R., Stassen, P., Tierney, J., Tripati, A., Wade, B., Westerhold, T., Witkowski, C., Zachos, J. C., Zhang, Y. G., Huber, M. and Lunt, D. J., 2019. The DeepMIP contribution to PMIP4: methodologies for selection, compilation and analysis of latest Paleocene and early Eocene climate proxy data, incorporating version 0.1 of the DeepMIP database. Geoscientific Model Development,12, 3149-3206. https://doi.org/10.5194/gmd-12-3149-2019.

Houben, A.J.P., Quaijtaal, W., Wade, B.S., Schouten, S. and Brinkhuis, H., 2019a. Organic-walled dinoflagellate cysts from the Eocene-Oligocene Transition in the Gulf of Mexico: indicators of climate- and sea-level change during the onset of Antarctic glaciation. Newsletters on Stratigraphy, 52 (2): 131-154. DOI: 10.1127/nos/2018/0455.

Houben, A.J.P., Bijl, P.K., Sluijs, A., Schouten, S., and Brinkhuis, H., 2019b. Late Eocene Southern Ocean cooling and invigoration of circulation preconditioned Antarctica for full-scale glaciation. Geochemistry, Geophysics, Geosystems, 20. https://doi.org/10.1029/2019GC008182.

Hsu, J. K., LaBrecque, J. L., et al. 1984. Initial Reports of the Deep- Sea Drilling Project, 73. Washington DC. US Government Printing Office, 798pp.

Hüneke, H. and Henrich, R. 2011. Pelagic Sedimentation in Modern and Ancient Oceans. In: Hüneke, H. and Mulder, T. Deep-sea sediments. Amsterdam, Elsevier. 215-351.

Hüneke, H. and Mulder, T. 2011. Deep-sea sediments. Amsterdam, Elsevier, 849 p.

Ivany, L.C., Van Simaeys, S., Domack, E.W., and Samson, S.D. 2006. Evidence for an earliest Oligocene ice sheet on the Antarctic Peninsula. Geology, 34(5), 377-380.

John, E.J., Pearson, P.N., Coxall, H.K., Birch, H., Wade, B.S. and Foster, G.L., 2013. Warm ocean processes and carbon cycling in the Eocene. Philosophical Transactions of the Royal Society A, 371: 20130099. http://dx.doi.org/10.1098/rsta.2013.0099

Kamatani A., 1982, Dissolution rates of silica from diatoms decomposing at various temperatures. Mar. Biol. 68, 91 – 96.

Kamikuri, S. and Wade, B.S., 2012. Radiolarian magnetobiochronology and faunal turnover across the middle/late Eocene boundary at Ocean Drilling Program Site 1052 in the western North Atlantic Ocean. Marine Micropaleontology, 88–89: 41–53.

Katz, M.E., Miller, K.G., Wright, J.D., Wade, B.S., Browning, J.V., Cramer, B.S. and Rosenthal, Y., 2008. Stepwise transition from the Eocene greenhouse to the Oligocene icehouse. Nature Geoscience, 1: 329-334.

Katz, M.E., Cramer, B.S., Toggweiler, J.R., Esmay, G., Liu, C., Miller, K.G., Rosenthal, Y., Wade, B.S. and Wright, J.D., 2011. Impact of Antarctic Circumpolar Current development on late Paleogene ocean structure. Science, 332: 1076-1079.

Kelly, D.C., Nielsen, T.M.J., McCarren, H.K.,, Zachos, J.C. and Ursula, R., 2010. Spatiotemporal patterns of carbonate sedimentation in the South Atlantic: Implications for carbon cycling during the Paleocene–Eocene thermal maximum: Palaeogeography, Palaeoclimatology, Palaeoecology, 293, 30-40, doi:10.1016/j.palaeo.2010.04.027

Kelly, D. C., T. M. J. Nielsen, and S. A. Schellenberg, 2012. Carbonate saturation dynamics during the Paleocene-Eocene thermal maximum: Bathyal constraints from ODP Sites 689 and 690 in the Weddell Sea (South Atlantic), Mar. Geol., 303–306, 75–86, doi:10.1016/j.margeo.2012.02.003.

Kennett, J.P. and Shackleton, N.J. 1976. Oxygen isotopic evidence for the development of the psychrosphere 38 Myr ago, Nature, 260, 513-515.

Kennett, J.P. and Stott, L.D., 1991, Abrupt deep-sea warming, palaeoceanographic changes and benthic extinctions at the end of the Paleocene: Nature, 353, 225-229, doi:10.1038/353225a0

Koch, P. L., J. C. Zachos, and P. D. Gingerich, 1992. Correlation between isotope records near the Palaeocene/Eoceneboundary, Nature, 358, 319–322.

Ladant, J.-B., Donnadieu, Y., Bopp, L., Lear, C. H., and Wilson, P. A., 2018. Meridional contrasts in productivity changes driven by the opening of Drake Passage. Paleoceanography and Paleoclimatology, 33. https://doi.org/10.1002/2017PA003211

Latimer, J.C., and Filippelli, G.M., 2002. Eocene to Miocene terrigenous inputs, paleoproductivity, and the onset of the ACC: geochemical evidence from ODP Leg 177, Site 1090. Palaeogeogr., Palaeoclimatol., Palaeoecol., 182:151-164.

Lazarus, D.B., 2011, The deep-sea microfossil record of macroevolutionary change in plankton and its study: Geological Society Special Publications, 358, 141-166, doi: 10.1144/SP358.10

Lazarus, D., Barron, J., Renaudie, J., Diver, P. and Turke, A., 2014, Cenozoic Planktonic Marine Diatom Diversity and Correlation to Climate Change: PLoS ONE, 9, doi: 10.1371/journal.pone.0084857

Leinen, M., Cwienk, D. Heath, G. R. Biscaye, P. E. Kolla, V. Thiede, J.and Dauphin, J. P., 1989, Distribution of biogenic silica and quartz in Recent deep-sea sediments: Geology, 14, 199–203.

Luciani, V., Giusberti, L., Agnini, C., Backman, J., Fornaciari, E. and Rio, D., 2007, The Paleocene–Eocene Thermal Maximum as recorded by Tethyan planktonic foraminifera in the Forada section (northern Italy): Marine micropaleontology, 64, 189-214.

Lyle, M., 2014. Deep-Sea Sediments. Encyclopedia of Marine Geosciences, 1-21.

Lyle, M., Wilson, P.A., Janecek, T.R., et al., 2002. Proceedings of the Ocean Drilling Program, Initial Results, 199: College Station, TX (Ocean Drilling Program).

Lyle, M., Barron, J., Bralower, T. J. Huber, M. Olivarez Lyle, A. Ravelo, A. C. Rea, D. K. and Wilson, P. A., 2008, Pacific Ocean and Cenozoic evolution of climate, Rev. Geophys., 46, RG2002, doi:10.1029/2005RG000190.

Mazzullo, J.M., Meyer, A., and Kidd, R.B. 1988. New sediment classification scheme for the Ocean Drilling Program. In Mazzullo, J.M., and Graham, A.G. (Eds.), Handbook for shipboard sedimentologists. Texas: Ocean Drilling Program, p. 45-67.

Meissener, K.J., Bralower, T.J., Alexander, K., Dunkley Jones, T., Sijp, W. and Ward, M., 2014, The Paleocene-Eocene Thermal Maximum: How much carbon is enough?: Paleoceanography, 29, 946-963, doi: 10.1002/2014PA002650

Miller, K.G., Wright, J.D., and Fairbanks, R.G. 1991. Unlocking the ice house: Oligocene-Miocene oxygen isotopes, eustasy, and margin erosion. Journal of Geophysical Research, 96, 6829-6848.

Miller, K.G., Browning, J.V., Aubry, M-P., Wade, B.S., Katz, M.E., Kulpecz, A.A., and Wright, J.D., 2008a. Eocene-Oligocene global climate and sea-level changes: St. Stephens Quarry, Alabama. Geological Society America Bulletin, 120 (1): 34-53.

Miller, K.G., Wright, J.D., Katz, M.E., Browning, J.V., Cramer, B.S., Wade, B.S., Misintseva, S.F. 2008b. A view of Antarctic ice-sheet evolution from sea-level and deep-sea isotope changes during the Late Cretaceous-Cenozoic. In: Cooper, A.K., Barrett, P.J., Stagg, H., Storey, B., Stump, E., Wise, W. and the 10th ISAES editorial team (Eds.). Antarctica: A keystone in a changing world. Proceedings of the 10th International Symposium on Antarctic Earth Sciences. The National Academies Press, Washington, D.C, pp. 55-70.

Miller, K.G., Wright, J.D., Katz, M.E., Wade, B.S., Browning, J.V., Cramer, B.S., and Rosenthal, Y., 2009. Climate threshold at the Eocene-Oligocene transition: Antarctic ice sheet influence on ocean circulation, In: Koeberl, C., and Montanari, A. (Eds.), The Late Eocene Earth—Hothouse, Icehouse, and Impacts: Geological Society of America Special Paper 452, p. 1–10, doi: 10.1130/2009.2452.

Moore, T.C. and Kamikuri S. 2012. Data report: Radiolarian stratigraphy across the Eocene/Oligocene boundary in the equatorial Pacific, Sites 1218, U1333, and U1334. In: Proceedings IODP, vol. 320/321, Pälike et al., Integr. Ocean Drill. Program Management International, Inc., Tokyo.

Moore, T.C., Rabinowitz, P.D., et al. 1984. Initial Reports of Deep Sea Drilling Project. US Government Printing Office, Washington, DC, USA, 74, 41-465.

Moore, T.C., Jr., Rea, D.K., Lyle, M. and Liberty, L.M., 2002. Equatorial ocean circulation in an extremely warm climate. Paleoceanography, 17 (1): 1005.

Moore, T. C., Jr., Backman, J., Raffi, I., Nigrini, C., Sanfilippo, A., Palike, H. and Lyle M. 2004. Paleogene tropical Pacific: Clues to circulation, productivity, and plate motion, Paleoceanography, 19, PA3013, doi:10.1029/2003PA000998.

Moore, T. C., Jr., Jarrard, R. D. Olivarez Lyle, A. and Lyle M. 2008. Eocene biogenic silica accumulation rates at the Pacific equatorial divergence zone,.Paleoceanography, 23, PA2202, doi:10.1029/2007PA001514.

Moore, T.C., Jr., Wade, B.S., Westerhold, T., Erhardt, A.M., Coxall, H.K., Baldauf, J. and Wagner, M., 2014. Equatorial Pacific productivity changes near the Eocene-Oligocene boundary. Paleoceanography, 29, 825-844. doi:10.1002/2014PA002656.

Muller, D., Sdrolias, M., Gaina, C., and Roest, W.R. 2008. Age, spreading rates, and spreading asymmetry of the world's ocean crust. Geochemistry, Geophysics, Geosystems, 9(4), Q04006.

Neori, A. and Holm-Hansen, O., 1982. Effect of temperature on rate of photosynthesis in Antarctic phytoplankton. Polar Biology, 1, 33-38, doi: 10.1007/BF00568752

Nicolo, M. J., Dickens, G. R. Hollis, C. J. and Zachos J. C., 2007. Multiple early Eocenehyperthermals: Their sedimentary expressionon the New Zealand continental marginand in the deep sea. Geology, 35, 699–702, doi:10.1130/G23648A.1.

Nunes, F., and Norris, R.D., 2006, Abrupt reversal in ocean overturning during the Paleocene/Eocene warm period: Nature, 439, 60-63, doi:10.1038/nature04386

Oreshkina, T.V., 2012, Evidence of Late Paleocene–Early Eocene hyperthermal events in biosiliceous sediments of western Siberia and adjacent areas: Australian Journal of Earth Sciences, 105, 145-153.

Oreshkina, T.V., and Radionova, E.P., 2014, Diatom record of the Paleocene-Eocene Thermal Maximum in marine paleobasins of Central Russia, Transuralia and adjacent regions. Nova Hedwigia, Beiheft, 143, 307-336.

Ouda, K., Berggren, W. and Sabour A.A., 2016, Upper Paleocene-Lower Eocene biostratigraphy of Darb Gaga, Southeastern Kharga Oasis Western Desert, Egypt: Journal of African Earth Sciences, 118, 12-23, doi: 10.1016/j.jafrearsci.2016.02.016

Pälike, C., Delaney, M.L. and Zachos, J.C., 2014, Deep-sea redox across the Paleocene-Eocene Thermal Maximum: Geochemistry, Geophysics, Geosystems, 15, 1038-1053, doi: 10.1002/2013GC005074

Pälike, H., Norris, R.D., Herrle, J.O., Wilson, P.A., Coxall, H.K., Lear, C.H., Shackleton, N.J., Tripati, A.K. and Wade, B.S. 2006. The heartbeat of the Oligocene climate system. Science, 314 (5807): 1894-1898.

Pälike et al. (64 co-authors), 2012. A Cenozoic record of the equatorial Pacific carbonate compensation depth. Nature, 488: 609-614.

Panchuk, K., Ridgewell, A. and Kump, R.L., 2008, Sedimentary response to Paleocene-Eocene Thermal Maximum carbon release: A model-data comparison: Geology, 36, 315-318, doi:10.1130/G24474A.1

Paytan, A., Averyt, K., Faul, K., Gray, E. and Thomas, E. 2007, Barite accumulation, ocean productivity, and Sr/Ba in barite across the Paleocene-Eocene Thermal Maximum: Geology, v. 35, p. 1139-1142.Pagani, M., Huber, M., Liu, Z., Bohaty, S.M., Henderiks, J., Sijp, W., Krishnan, S., and DeConto, R.M. 2011. The role of carbon dioxide during the onset of Antarctic glaciation. Science, 334, 1261-1264,

Pearson, P.N., McMillan, I.K., Wade, B.S., Dunkley Jones, T., Coxall, H.K., Bown, P.R. and Lear, C.H., 2008. Extinction and environmental change across the Eocene-Oligocene boundary in Tanzania. Geology, 36 (2): 179-182.

Pearson, P.N., Foster, G.L., and Wade, B.S. 2009. Atmospheric carbon dioxide through the Eocene-Oligocene climate transition. Nature, 461, 1110-1113.

Penman, D. E., 2016, Silicate weathering and North Atlantic silica burial during the Paleocene-Eocene Thermal Maximum: Geology, 44(9), 731–734, https://doi.org/10.1130/G37704.1

Penman, D.E., Honisch, B., Zeebe, R.E., Thomas, E. and Zachos, J.C., 2014, Rapid and sustained surface ocean acidification during the Paleocene-Eocene Thermal Maximum: Paleoceanography, 29, 357-369, doi: 10.1002/2014PA002621

Penman, D. E., Keller, A., D'haenens, S., Kirtland Turner, S., and Hull, P. M. 2019. Atlantic deep-sea cherts associated with Eocene hyperthermal events. Paleoceanography and Paleoclimatology, 34, 287–299. https://doi.org/10.1029/2018PA003503.

Peterson, L.C., Murray, D.W., Ehrmann, W.U., and Hempel, P. 1992. Cenozoic carbonate accumulation and compensation depth changes in the Indian Ocean. In: Duncan R.A., Rea, D.K., Kidd, R.B., von Rad, U., and Weissel, J.K. (eds.). Synthesis of Results from

Scientific Drilling in the Indian Ocean. Washington DC, USA, American Geophysical Union, 471-475. (AGU Geophysical Monograph 70).

Petrou, K., Baker, K.G., Nielsen, D.A., Hancock, A.M., Schulz, K.G. and Davidson, A.T., 2019. Acidification diminishes diatom silica production in the Southern Ocean. Nature Climate Change, 9, 781-786.

Pfuhl, H. A. and McCave, I. N., 2005. Evidence for late Oligocene establishment of the Antarctic Circumpolar Current. Earth and Planetary Science Letters 235, 715–728.

Plancq, J., Mattioli, E., Pittet, B., Simon, L., and Grossi, V. 2014. Productivity and sea-surface temperature changes recorded during the late Eocene-early Oligocene at DSDP Site 511 (South Atlantic). Paleogeography, Palaeoclimatology, Palaeoecology, 407, 34-44.

Prothero, D.R. and Berggren, W.A. (eds.). 1992. Eocene-Oligocene Climactic and Biotic Evolution. Princeton, Princeton University Press.

Rabosky, D.L. and Sorhannus, U., 2009. Diversity dynamics of marine plantonic foramtoms across the Cenozoic. Nature, 457: 183-186.

Ragueneau, O. Tréguer, P. Leynaert, A. Anderson, R.F. Brzezinski, M.A. DeMaster, D.J. Dugdale, R.C. Dymond, J. Fischer, G. François, R. Heinze, C. Maier-Reimer, E. Martin- Jézéquel, V. Nelson, D.M., and Quéguiner, B. 2000. A review of the Si cycle in the modern ocean: recent progress and missing gaps in the application of biogenic opal as a paleoproductivity proxy. Global and Planetary Change, 26(4), 317-365.

Rea, D.K. and Lyle, M.W. 2005. Paleogene calcite compensation depth in the eastern subtropical Pacific: Answers and questions. Paleoceanography, v. 20, PA1012.

Rea, D.K., Lyle, M.W., Liberty, L.M., Hovan, S.A., Bolyn, M.P., Gleason, J.D., Hendy, I.L., Latimer, J.C., Murphy, B.M., Owen, R.M., Paul, C.F., Rea, T.H.C., Stancin, A.M., and

Thomas, D.J., 2006, Broad region of no sediment in the southwest Pacific Basin: Geology, v. 34, p. 873–876, doi: 10.1130/G22864.1.

Renaudie, J., 2016. Quantifying the Cenozoic marine diatom deposition history: links to the C and Si cycles. Biogeosciences, 13: 6003-6014.

Röhl, U, Norris, R.D. and Ogg, J.G., 2003. Cyclostratigraphy of upper Paleocene and late Eocene sediments at Blake Nose Site 1051 (western North Atlantic). In: Gingerich, P, Schmitz, B, Thomas, E and Wing, S (eds.) Causes and Consequences of Globally Warm Climates in the Early Paleogene. Geological Society of America (GSA) Special Paper Series, 567-588. doi:10.1130/0-8137-2369-8.567

Salamy, K. A. and Zachos, J. C. 1999. Latest Eocene-Early Oligocene climate change and Southern Ocean fertility: inferences from sediment accumulation and stable isotope data. Palaeogeography, Palaeoclimatology, Palaeoecology, 145(1), 61-77.

Sanfilippo, A. and Blome, C.D. 2001. Biostratigraphic implications of mid-latitude Palaeocene-Eocene radiolarian faunas from Site 1051A, ODP Leg 171B, Blake Nose, western North Atlantic. In: Kroon, D., Norris, R. D. and Klaus, A. (Eds.). Western North Atlantic Palaeogene and Cretaceous Palaeoceanography. Geological Society of London Special Publications, 183: 185-224

Saunders, A.D., 2016, Two LIPs and two Earth-system crises: the impact of the North Atlantic Igneous Province and the Siberian Traps on the Earth-surface carbon cycle: Geological Magazine, 153, 201-222, doi: 10.1017/S0016756815000175

Scher, H.D. and Martin, E.E., 2006. Timing and climatic consequences of the opening of Drake Passage. Science, 312, 428-430.

Scher, H.D., Bohaty, S.M., Smith, B.W. and Munn, G.H. 2014. Isotopic interrogation of a suspected late Eocene glaciation. Paleoceanography, 29, 628-644

Scher, H. D., Whittaker, J.M., Williams, S.E., Latimer, J.C., Kordesch, W.E.C. and Delaney, M.L., 2015. Onset of Antarctic Circumpolar Current 30 million years ago as Tasmanian Gateway aligned with westerlies. Nature 523, 580–583.

Schulte, P., Wade, B.S., Kontny, A., and Self-Trail, J.M., 2009. The Eocene-Oligocene sedimentary record in the Chesapeake Bay impact structure: Implications for climate and sea level changes on the western Atlantic margin. In: Gohn, G.S., Koeberl, C., Miller, K.G., and Reimold, W.U., (Eds.), The ICDP-USGS Deep Drilling Project in the Chesapeake Bay Impact Structure: Results from the Eyreville Core Holes: Geological Society of America Special Papers 458: 839-865. doi: 10.1130/2009.2458(35).

Self-Trail, J.M., Robinson, M.M., Bralower, T.J., Sessa, J.A., Hajek, E.A., Kump, L.R.,Trampush, S.M., Willard, D.A., Edwards, L.E., Powars, D.S., Wandless, G.A., 2017. Shallow marine response to global climate change during the Paleocene-EoceneThermal Maximum, Salisbury Embayment, USA. Paleoceanography 32, 710–728.

Seton, M., Muller, R.D., Zahirovic, S., Gaina, C., Shephard, G., Talsma, A., Gurnis, M., Turner, M., Maus, S. and Chandler, M., 2012, Global continental and ocean basin reconstructions since 200 Ma: Earth-Science Reviews, 113, 212-270.

Shipboard Scientific Party, 1996. Site 959. In Mascle, J., Lohmann, G.P., Clift, P.D., et al., Proc. ODP, Init. Repts., 159: College Station, TX (Ocean Drilling Program), 65–150. doi:10.2973/odp.proc.ir.159.105.1996

Siever, R., 1957. The Silica Budget in the Sedimentary Cycle. American Mineralogist, 42, 821–841.

Sims, P.A., Mann, D.G., Medlin, L.K., 2006, Evolution of the diatoms: insights from fossil, biological and molecular data. Phycologia, 45, 361-402.

Stickley, C. E., H. Brinkhuis, S. A. Schellenberg, A. Sluijs, U. Ro¨hl, M. Fuller, M. Grauert, M. Huber, J. Warnaar, and G. L. Williams, 2004, Timing and nature of the deepening of the Tasmanian Gateway, Paleoceanography, 19, PA4027, doi:10.1029/2004PA001022

Takahashi, T., Broecker, W.S., 1977. Mechanisms for calcite dissolution on the sea floor. In: The Fate of Fossil Fuel CO2 in the Oceans. In: Anderson, N.R., Malahoff, A. (Eds.), Marine Science, vol., 6. Plenum, New York, 455-477.

Thomas, E., and Shackleton, N. J., 1996. The Palaeocene-Eocene benthic foraminiferal extinction and stable isotope anomalies. Geological Society London Special Publication, 101: 401-441.

van Andel, T.H., 1975, Mesozoic/Cenozoic calcite compensation depth and the global distribution of calcareous sediments: Earth and Planetary Science Letters, 26, 187-194.

van Andel, T.H., and Moore, T. C. JR. 1974 Cenozoic calcium carbonate distribution and calcite compensation depth in the central equatorial Pacific. Geology, 2, 87-92.

Wade, B.S. and Pearson, P.N., 2008. Planktonic foraminiferal turnover, diversity fluctuations and geochemical signals across the Eocene/Oligocene boundary in Tanzania. Marine Micropaleontology, 68: 244-255.

Wade, B.S., Pearson, P.N., Berggren, W.A. and Pälike, H., 2011. Review and revision of Cenozoic tropical planktonic foraminiferal biostratigraphy and calibration to the geomagnetic polarity and astronomical time scale. Earth Science Reviews, 104: 111-142.

Wade, B.S., Houben, A.J.P., Quaijtaal, W., Schouten, S., Rosenthal, Y., Miller, K.G., Katz, M.E., Wright, J.D. and Brinkhuis, H., 2012. Multiproxy record of abrupt sea surface cooling across the Eocene-Oligocene transition in the Gulf of Mexico. Geology, 40 (2): 159-162.

Wade, B.S., Pearson, P.N., Olsson, R.K., Premoli Silva, I., Berggren, W.A., Spezzaferri, S., Huber, B.T., Coxall, H.K., Premec-Fucek, V., Hernitz Kucenjak, M., Hemleben, Ch., Leckie, R.M., and Smart, C.W., 2018, Taxonomy, biostratigraphy, phylogeny, and diversity of Oligocene and early Miocene planktonic foraminifera, in Wade, B.S., Olsson, R.K., Pearson, P.N., Huber, B.T. and Berggren, W.A., Atlas of Oligocene Planktonic Foraminifera, Cushman Foundation of Foraminiferal Research, Special Publication, No. 46, p. 11-28.

Westerhold, T., Röhl, U., Frederichs, T., Agnini, C., Raffi, I., Zachos, J. C., and Wilkens, R. H., 2017. Astronomical calibration of the Ypresian timescale: implications for seafloor spreading rates and the chaotic behavior of the solar system?, Clim. Past, 13, 1129–1152, https://doi.org/10.5194/cp-13-1129-2017.

Winguth, A., Ellen, T. and Winguth, C., 2012, Global decline in ocean ventilation, oxygenation, and productivity during the Paleocene-Eocene thermal maximum: Implications for the benthic extinction: Geology, 40, 263-266, doi: 10.1130/G32529.1

Wise, S.W. Jr., Breza, J.R., Harwood, D.M., Wei, W., Zachos, J., 1991. Paleogene glacial history of Antarctica, in: McKenzie, J.A., Weissert, H., (Eds.), Controversies in modern geology; evolution of geological theories in sedimentology, Earth history and tectonics. London: Academic Press, pp. 133–171

Wise, S.W., Breza, J.R., Harwood, D.M., Wei, W., and Zachos, J.C., 1992. Paleogene glacial history of Antarctica in light of Leg 120 drilling results. In Wise, S.W., Schlich, R., et al., Proc. ODP, Sci. Results, 120: College Station, TX (Ocean Drilling Program), 1001-1030.

Witkowski, J., Penman, D.E., Bryłka, K., Wade, B.S., Matting, S., Harwood, D.M., and Bohaty, S.M., 2020a. Early Paleogene biosiliceous sedimentation in the Atlantic

Ocean: Testing the inorganic origin hypothesis for Paleocene and Eocene chert and porcellanite. Palaeogeography, Palaeoclimatology, Palaeoecology, 556, 109896. doi:10.1016/j.palaeo.2020.109896

Witkowski, J., Harwood, D.M., Wade, B.S. and Brylka, K., 2020b. Rethinking the chronology of early Paleogene sediments in the western North Atlantic using diatom biostratigraphy. Marine Geology, 424, 106168.

Zachos, J.C., Breza, J., and Wise, S.W. 1992. Early Oligocene ice sheet expansion on Antarctica: Sedimentological and isotopic evidence from Kerguelen Plateau. Geology, 20, 569-573.

Zachos, J. C., Quinn, T. M., and Salamy, K. A. 1996. High-resolution (104 years) deep-sea foraminiferal stable isotope records of the Eocene-Oligocene climate transition. Paleoceanography, 11(3), 251-266.

Zachos, J.C., Rohl, U., Schellenberg, S.A., Sluijs, A., Hodell, D.A., Kelly, D.C., Thomas, E., Nicolo, M., Raffi, I., Lourens, L.J., McCarren, H. and Kroon, D., 2005, Rapid Acidification of the Ocean During the Paleocene-Eocene Thermal Maximum: Science, 308, 1611-1615, doi: 10.1126/science.1109004

Zanazzi, A., Kohn, M.J., MacFadden, B.J., and Terry, D.O., Jr., 2007, Large temperature drop across the Eocene–Oligocene transition in central North America: Nature, 445, 639–642, doi:10.1038/nature05551.

Zeebe, R.E. and Zachos, J.C., 2007, Reversed deep-sea carbonate ion basin gradient during Paleocene-Eocene thermal maximum: Paleoceanography, 22, doi: 10.1029/2006PA001395

Zeebe, R.E., Zachos, J.C., Dickens, G.R., 2009. Carbon dioxide forcing alone insufficient to explain Palaeocene–Eocene Thermal Maximum warming. Nat. Geosci. 2, 576–580. doi:10.1038/ngeo578

Zhang, Q., Willems, H. and Ding, L., 2013. Evolution of the Paleocene-Early Eocene larger benthic foraminifera in the Tethyan Himalaya of Tibet, China: International Journal of Earth Sciences, 102, 1427-1445.

TABLE CAPTIONS

Table 1. Modern deep-sea sediment lithologies.

Table 2. Upper Paleocene and PETM deep-sea sediment lithologies from DSDP, ODP and IODP sites.

Table 3. Upper Eocene and lower Oligocene deep-sea sediment lithologies from DSDP, ODP and IODP sites.